Title

Neuroanatomical and Functional Dissociations between Variably Present Anterior Lateral Prefrontal Sulci.

Journal

Journal of Cognitive Neuroscience, 35(11)

Authors

Weiner, Kevin
Willbrand, Ethan
Bunge, Silvia

Publication Date

2023-11-01

DOI

10.1162/jocn_a_02049

Peer reviewed

Neuroanatomical and Functional Dissociations between Variably Present Anterior Lateral Prefrontal Sulci

Ethan H. Willbrand[1,2], Silvia A. Bunge[1*], and Kevin S. Weiner[1*]

Abstract

■ The lateral prefrontal cortex (LPFC) is an evolutionarily expanded region in humans that is critical for numerous complex functions, many of which are largely hominoid specific. Although recent work shows that the presence or absence of specific sulci in anterior LPFC is associated with cognitive performance across age groups, it is unknown whether the presence of these structures relates to individual differences in the functional organization of LPFC. To fill this gap in knowledge, we leveraged multimodal neuroimaging data from two samples encompassing 82 young adult humans (aged 22–36 years) and show that the dorsal and ventral components of the paraintermediate frontal sulcus, or pimfs, present distinct morphological (surface area), architectural (thickness and myelination), and functional (resting-state connectivity networks) properties. We further contextualize the pimfs components within classic and modern cortical parcellations. Taken together, the dorsal and ventral pimfs components mark transitions in LPFC anatomy and function, across metrics and parcellations. These results emphasize that the pimfs is a critical structure to consider when examining individual differences in the anatomical and functional organization of LPFC and suggest that future individual-level parcellations could benefit from incorporating sulcal anatomy when delineating LPFC cortical regions. ■

INTRODUCTION

A main goal in cognitive and systems neuroscience is to precisely understand how the human cerebral cortex is organized morphologically, anatomically, and functionally. Of particular interest are association cortices, which have expanded the most throughout evolution and present anatomical and functional features that are cognitively relevant—some of which are unique to humans. For example, classic and ongoing work shows that the lateral prefrontal cortex (LPFC) displays a complex structural and functional organization that supports numerous complex cognitive abilities (Demirtaş et al., 2019; Nee & D'Esposito, 2016; Stuss & Knight, 2013; Badre & D'Esposito, 2009; Petrides, 2005; Levy & Goldman-Rakic, 2000; Rosenkilde, 1979). A growing body of recent work demonstrates the utility of studying small, shallow, and variable sulci (often referred to as tertiary sulci; Armstrong, Schleicher, Omran, Curtis, & Zilles, 1995; Welker, 1990; Chi, Dooling, & Gilles, 1977; Sanides, 1964) for understanding the anatomical and functional organization of association cortices, including LPFC (Willbrand, Parker, et al., 2022; Amiez et al., 2013, 2021; Miller, D'Esposito, & Weiner, 2021; Miller, Voorhies, Lurie, D'Esposito, & Weiner, 2021; Troiani, Patti, & Adamson, 2020; Lopez-Persem, Verhagen, Amiez, Petrides, & Sallet, 2019; Weiner, 2019; Troiani, Dougherty, Michael, & Olson, 2016; Li, Sescousse, Amiez, & Dreher, 2015; Amiez & Petrides, 2014; Sanides, 1964). Intriguingly, some tertiary sulci are present in every brain, whereas others are not (Hathaway et al., 2023; Vallejo-Azar et al., 2022; Willbrand, Parker, et al., 2022; Willbrand, Voorhies, Yao, Weiner, & Bunge, 2022; Miller, Voorhies, et al., 2021; Miller et al., 2020; Nakamura, Nestor, & Shenton, 2020; Amiez et al., 2019; Petrides, 2019; Malikovic et al., 2012; Paus et al., 1996). In the present study, we focus on the morphological, architectural, and functional features of variably present sulci in anterior LPFC—the dorsal (pimfs-d) and ventral (pimfs-v) components of the paraintermediate frontal sulcus (pimfs), respectively. We do so for four main reasons.

First, the anterior and posterior LPFC differ based on incidence rates of the small, shallow, and variable tertiary sulci located within them. Across age groups, posterior LPFC contains three tertiary sulci that are present in all participants (Yao, Voorhies, Miller, Bunge, & Weiner, 2022; Miller, Voorhies, et al., 2021; Voorhies, Miller, Yao, Bunge, & Weiner, 2021). By contrast, in anterior LPFC, a given hemisphere can have (i) a pimfs-d and pimfs-v; (ii) a pimfs-d, but not a pimfs-v (or vice versa); or (iii) neither component (Willbrand, Jackson, et al., 2023; Willbrand, Voorhies, et al., 2022). Second, the sulcal depth of a subset of these posterior and anterior LPFC sulci are related to cognitive performance (Yao et al., 2022; Voorhies et al., 2021). Third, two separate studies in pediatric and adult cohorts show that the presence or absence of the pimfs

[1]University of California Berkeley, [2]University of Wisconsin–Madison
*Co-senior authorship.

Journal of Cognitive Neuroscience 35:11, pp. 1846–1867
https://doi.org/10.1162/jocn_a_02049

is related to reasoning performance (Willbrand, Jackson, et al., 2023; Willbrand, Voorhies, et al., 2022). Fourth, although our prior work indicated that the three posterior LPFC sulci are anatomically distinct structures that co-localize with distinct functional networks (Miller, Voorhies, et al., 2021), the anatomical and functional distinctiveness and relevance of the pimfs components have yet to be investigated.

To fill this gap in knowledge, we tested whether the two pimfs components are functionally and/or anatomically dissociable using classic criteria (Van Essen, 2003; Kaas, 1997; Felleman & Van Essen, 1991) and in line with our prior work in posterior LPFC (Miller, Voorhies, et al., 2021) via a three-pronged approach in 72 participants from the Human Connectome Project (HCP; 144 hemispheres; 249 pimfs labels; 50% female, aged 22–36 years). First, we extracted and compared the morphological (depth, surface area) features of the pimfs components. Second, we did the same for architectural (gray matter thickness, myelination) features of the pimfs. Third, we created functional connectivity profiles for each pimfs component using functional network parcellations of the human cerebral cortex unique to each HCP participant that was created blind to cortical folding and our sulcal definitions (Kong et al., 2019). Finally, we contextualized the alignment of our individual-level pimfs labels with several widely used group-level modern and classic parcellations of the human cerebral cortex spanning multiple cortical features.

METHODS

Multimodal HCP Data Set

Data for the young adult human cohort analyzed in the present study were taken from the HCP database: ConnectomeDB (db.humanconnectome.org). Here, as in several prior studies (Willbrand, Ferrer, Bunge, & Weiner, 2023; Willbrand, Jackson, et al., 2023; Willbrand, Maboudian, et al., 2023; Willbrand, Parker, et al., 2022; Miller, Voorhies, et al., 2021), we used a randomly selected subset of 72 participants (50% female, aged between 22 and 36 years), given the time-intensive process of individual sulcal labeling. In addition, previous work examining structural-functional correspondences in individual hemispheres shows that this sample size is large enough to encapsulate individual differences and detect reliable effects in individual hemispheres (e.g., as few as 20 hemispheres is typically considered a sufficient sample size; Amunts, Mohlberg, Bludau, & Zilles, 2020; Lopez-Persem et al., 2019; Zlatkina, Amiez, & Petrides, 2016; Amunts & Zilles, 2015; Amiez, Kostopoulos, Champod, & Petrides, 2006). HCP consortium data were previously acquired using protocols approved by the Washington University Institutional Review Board, and informed consent was obtained from all participants.

Anatomical T1-weighted (T1-w) MRI scans (0.7-mm voxel resolution) were obtained in native space from the HCP database, along with outputs from the HCP modified FreeSurfer pipeline (v5.3.0; Glasser et al., 2013; Dale, Fischl, & Sereno, 1999; Fischl, Sereno, & Dale, 1999; Fischl, Sereno, Tootell, & Dale, 1999). Additional details on image acquisition parameters and image processing can be found in the previously published work by Glasser and colleagues (2013). Maps of the ratio of T1-w and T2-w scans, which is a measure of tissue contrast enhancement related to myelin content, were downloaded as part of the HCP Structural Extended release. All subsequent sulcal labeling and extraction of anatomical metrics were calculated on the cortical surface reconstructions of individual participants generated through the HCP's custom-modified version of the FreeSurfer pipeline (Glasser et al., 2013; Dale et al., 1999; Fischl, Sereno, & Dale, 1999; Fischl, Sereno, Tootell, et al., 1999).

Anatomical Analyses

Manual Sulcal Labeling

LPFC sulci were manually defined within each individual hemisphere using *tksurfer*, as in prior work (Willbrand, Ferrer, et al., 2023; Willbrand, Jackson, et al., 2023; Willbrand, Voorhies, et al., 2022; Yao et al., 2022; Miller, Voorhies, et al., 2021; Voorhies et al., 2021). Manual lines were drawn on the inflated cortical surface to define sulci based on the most recent definitions of pimfs and sulcal patterning in LPFC by Petrides (2019), as well as by the *pial* and *smoothwm* surfaces of each individual (Miller, Voorhies, et al., 2021). In some cases, the precise start- or end point of a sulcus can be difficult to determine on a surface (Borne, Rivière, Mancip, & Mangin, 2020). Thus, using the inflated, *pial*, and *smoothwm* surfaces to inform our labeling allowed us to form a consensus across surfaces and clearly determine each sulcal boundary. The location of pimfs components was confirmed by trained independent raters and finalized by a neuroanatomist (K. S. W.).

In the present study, we restricted our analyses to the anterior MFG (aMFG; Figure 1), as the anatomical and functional properties of the tertiary sulci in posterior MFG (pMFG) have already been assessed (Miller, Voorhies, et al., 2021). Although this project focused primarily on the pimfs and three immediately surrounding sulci (i.e., the horizontal component of the intermediate middle frontal sulcus [imfs-h], ventral component of the intermediate middle frontal sulcus [imfs-v], and inferior frontal sulcus [ifs]), the manual identification of the other 19 LPFC sulci (2985 sulcal definitions across all 72 participants) was required to ensure the most accurate definition of all sulci. For in-depth descriptions of all LPFC sulci, see Willbrand, Ferrer, and colleagues (2023); Willbrand, Jackson, and colleagues (2023); Yao and colleagues (2022); Miller, D'Esposito, and colleagues (2021); Miller, Voorhies, and colleagues (2021); Voorhies and colleagues (2021); and Petrides (2019). In each hemisphere, we first labeled the

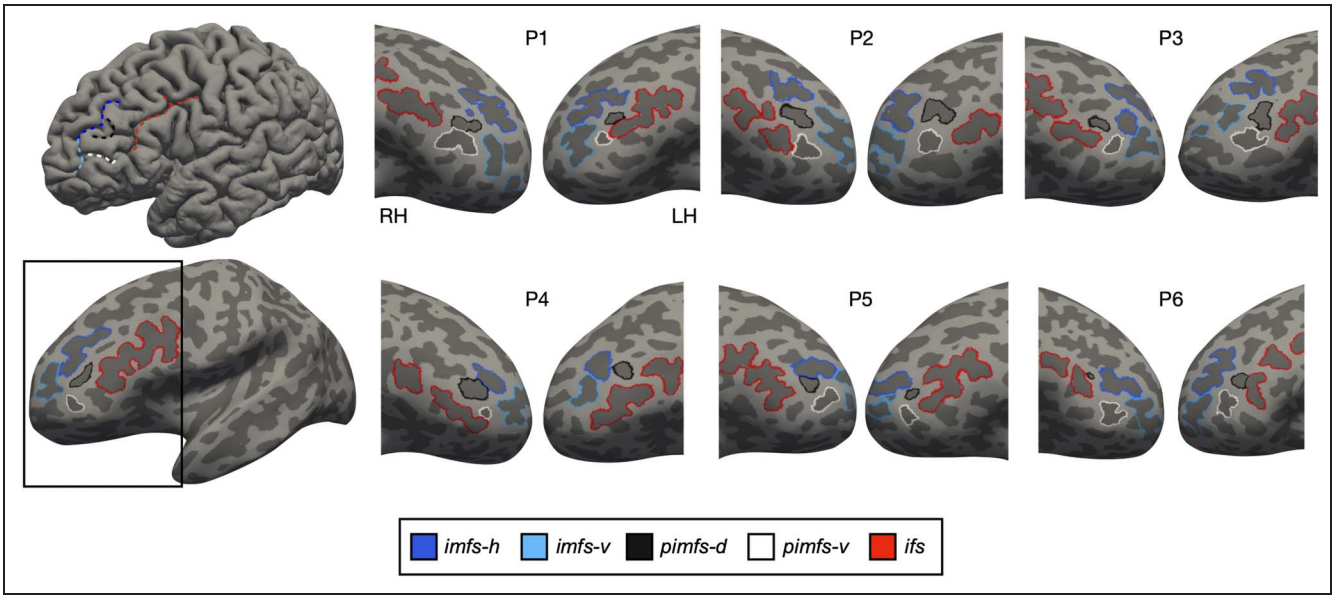

Figure 1. Components of the paraintermediate frontal sulcus are often, but not always, identifiable within individual hemispheres. Left: pial (top) and inflated (bottom) left hemisphere (dark gray: sulci; light gray: gyri) from an example participant with the two components of the paraintermediate frontal sulcus (dorsal: pimfs-d; ventral: pimfs-v) defined, as well as three prominent surrounding sulci: (i) horizontal component of the intermediate frontal sulcus (imfs-h), (ii) ventral component of the intermediate frontal sulcus (imfs-v), and (iii) inferior frontal sulcus (ifs). Sulci are colored according to the legend below. The black box around the inflated surface focuses on the LPFC. Right: Additional left (LH) and right (RH) inflated cortical surfaces of six individual participants focused on the LPFC. Although there can be 0, 1, or 2 pimfs components in a given hemisphere, we primarily show hemispheres containing two components (with the exception of P4). Fifty-seven percent of individuals had both components in both hemispheres.

three surrounding prominent sulci (ifs, imfs-h, and imfs-v) so that we could use them as landmarks to identify the pimfs (Figure 1). As described in prior work (Willbrand, Jackson, et al., 2023; Willbrand, Voorhies, et al., 2022; Petrides, 2013, 2019), the dorsal and ventral components of the pimfs (pimfs-d and pimfs-v) were generally defined using the following twofold criterion: (i) the sulci ventrolateral to the imfs-h and imfs-v, respectively, and (ii) superior and/or anterior to the mid-anterior portion of the ifs (Figure 1).

Quantifying and Comparing the Morphology and Architecture of the Paraintermediate Frontal Sulcus Components

Morphologically, we compared the depth and surface area of the pimfs components, as these are two of the primary morphological features used to define and characterize sulci (Willbrand, Ferrer, et al., 2023; Li et al., 2022; Willbrand, Parker, et al., 2022; Willbrand, Voorhies, et al., 2022; Yao et al., 2022; Miller, D'Esposito, et al., 2021; Miller, Voorhies, et al., 2021; Natu et al., 2021; Voorhies et al., 2021; Miller et al., 2020; Lopez-Persem et al., 2019; Madan, 2019; Petrides, 2019; Weiner, 2019; Weiner, Natu, & Grill-Spector, 2018; Weiner et al., 2014; Armstrong et al., 1995; Welker, 1990; Chi et al., 1977; Sanides, 1964). We expected that the pimfs components would be shallower and smaller than the three more prominent sulci surrounding them, based on our prior work on the three pMFG tertiary sulci in young adults (Miller, Voorhies, et al., 2021) and for the pimfs in children and adolescents (Voorhies et al., 2021). Indeed, this is what we found (Appendix and Figure A1).

Sulcal depth and surface area were measured following the same procedures as in our prior work (Yao et al., 2022; Voorhies et al., 2021). Mean sulcal depth values (in standard FreeSurfer units) were computed in native space from the .sulc file generated in FreeSurfer (Dale et al., 1999; Fischl, Sereno, & Dale, 1999; Fischl, Sereno, Tootell, et al., 1999) with custom Python code (leveraging functions from the *nilearn* and *nibabel* packages) developed in our prior work (Voorhies et al., 2021). Briefly, depth values are calculated based on how far removed a vertex is from what is referred to as a "mid-surface," which is determined computationally such that the mean of the displacements around this "mid-surface" is zero. Thus, generally, gyri have negative values, whereas sulci have positive values. Given the shallowness and variability in the depth of tertiary sulci (Yao et al., 2022; Miller, Voorhies, et al., 2021; Voorhies et al., 2021), some mean depth values extend below zero. We emphasize that this just reflects the metric implemented in FreeSurfer. Each depth value was also normalized by the deepest point in the given hemisphere. Surface area (in square millimeters) was generated for each sulcus through the *mris_anatomical_stats* function in FreeSurfer (Fischl & Dale, 2000). Surface area was normalized by hemispheric surface area as in our prior work (Hathaway et al., 2023; Willbrand, Ferrer, et al., 2023; Willbrand, Maboudian, et al., 2023; Willbrand, Voorhies, et al., 2022).

Architecturally, we compared cortical thickness and myelination (Figure 2A), as in our prior work (Willbrand, Parker, et al., 2022; Miller, Voorhies, et al., 2021; Voorhies et al., 2021). Mean gray matter cortical thickness (mm) was extracted from each sulcus using the *mris_anatomical_stats* function in FreeSurfer (Fischl & Dale, 2000). To quantify myelin content, we used an in vivo proxy of myelination: the T1-w/T2-w maps for each individual hemisphere (Shams, Norris, & Marques, 2019; Glasser & Van Essen, 2011). To generate the T1-w/T2-w maps, two T1-w and T2-w structural magnetic resonance scans from each participant were registered together and averaged as part of the HCP processing pipeline (Glasser et al., 2013). The averaging helps to reduce motion-related effects or blurring. In addition, the T1-w/T2-w images were bias-corrected for distortion effects using field maps, as described by Glasser and colleagues (Glasser et al., 2013). We then extracted the average T1-w/T2-w ratio values across each vertex for each sulcus using custom Python code, leveraging functions from the *nilearn* and *nibabel* packages (Miller, Voorhies, et al., 2021).

To assess whether these four metrics differed between the pimfs components, we ran a repeated-measures ANOVA (rm-ANOVA) with the following factors: Sulcal Component (pimfs-d and pimfs-v) × Metric (surface area, depth, cortical thickness, and myelination) × Hemisphere (left and right). We also assessed whether the presence/absence of the pimfs-d impacted these features of the pimfs-v, and vice versa, by running another rm-ANOVA for each component, exchanging the predictor Sulcal Component for Number of Components (one, two). We also implemented a similar analysis to compare the pimfs components with the prominent neighboring sulci (Appendix and Figure A1).

Functional Analyses

To assess whether the pimfs components are functionally distinct, we implemented a three-pronged approach leveraging data spanning the individual (Kong et al., 2019; Gordon, Laumann, Gilmore, et al., 2017) and group levels (Foit et al., 2022; Scholtens, de Reus, de Lange, Schmidt, & van den Heuvel, 2018; Fan et al., 2016; Glasser et al., 2016; Van Essen, 2005), which we now discuss in turn.

Individual Level: Comparing Connectivity of the Paraintermediate Frontal Sulcus Components from Resting-state Functional Connectivity Network Parcellations

To determine whether the pimfs components are functionally distinct, we generated functional connectivity profiles using a recently developed analytic approach (Willbrand, Parker, et al., 2022; Miller, Voorhies, et al., 2021). First, we used resting-state network parcellations

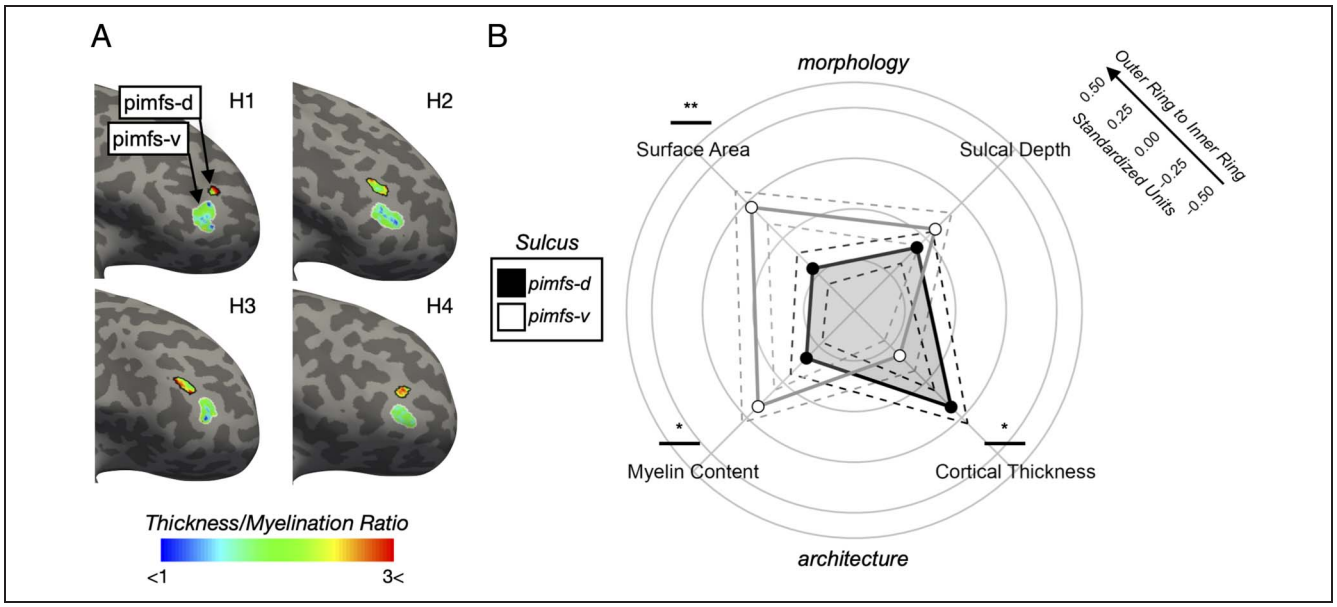

Figure 2. Pimfs-d is 15.73% smaller, 2.48% cortically thicker, and 0.81% less myelinated on average than pimfs-v. (A) Four example inflated hemispheres (labeled H1, H2, etc.; two left and two right; all oriented as right hemispheres) displaying the thickness/myelination ratio (heatmap; see bottom color bar) within each pimfs component (pimfs-d: black outline; pimfs-v: white outline). Surfaces are focused on LPFC as in Figure 1. Note that these example hemispheres display the effects shown in (B): The pimfs-d is smaller, as well as thicker and less myelinated (as shown by the higher thickness/myelination ratio) than the pimfs-v. (B) Polar plot showing the mean morphological (top) and architectural (bottom) values for the pimfs components (averaged across hemispheres; Figure A2 for these values separated by hemisphere). The units shown to the right correspond with the value of each concentric ring (topmost unit: outer ring; bottom unit: innermost ring). These units are standardized (across components and hemispheres for each metric) to allow for these metrics to be plotted together. Solid lines and dots represent the means. Dashed lines represent ± standard error. Lines and dots are colored by sulcal component (pimfs-d: black, pimfs-v: white/gray). Line and asterisks above each of the metric labels indicate the post hoc pairwise comparisons on the Sulcus × Metric interaction (*$p < .05$, **$p < .01$).

for each individual participant from Kong and colleagues (2019), who previously generated individual network definitions by applying a hierarchical Bayesian network algorithm to produce maps for each of the 17 networks in individual HCP participants. These data were calculated in the template HCP *fs_LR* 32 k space. Importantly, this parcellation was conducted blind to cortical folding (and therefore, also blind to our sulcal definitions). Next, we resampled the network profiles for each participant onto the *fsaverage* cortical surface and then to each native surface using CBIG tools (https://github.com/ThomasYeoLab/CBIG).

We then calculated, for each hemisphere and participant, the spatial overlap between a sulcus and each of the (i) eight main networks comprising the parcellation (auditory, control, default, dorsal attention, somatomotor, temporal–parietal, ventral attention, and visual) and (ii) 17 individual resting-state networks (i.e., considering subnetworks: auditory, Control A, Control B, Control C, Default A, Default B, Default C, Dorsal Attention A, Dorsal Attention B, Somatomotor A, Somatomotor B, temporal–parietal, Ventral Attention A, Ventral Attention B, Visual A, Visual B, Visual C). To quantify the overlap between a sulcus and each of the networks, we computed Dice coefficients:

$$DICE(X,Y) = \frac{2|X \cap Y|}{|X| + |Y|}$$

where X and Y are the sulcus and network, $||$ represents the number of elements in each set, and $\cap$ represents the intersection of two sets. Fourth, we ran two rm-ANOVAs (factors: Sulcal Component [pimfs-d and pimfs-v] × Network [8 or 17 networks] × Hemisphere [left and right]) to determine whether the network profiles (i.e., the Dice coefficient overlap with each network) of the pimfs-d and pimfs-v were differentiable from one another. In the first rm-ANOVA, we compared the profiles using the general eight networks to assess broad correspondences. Next, we compared the overlap of the pimfs components with all 17 networks to determine which subnetworks were driving the effect in the first model.

To quantify variability and individual differences in the overlap with these functional networks for each pimfs component, we calculated the Wasserstein metric (Earth Mover's Distance) between the resting-state network overlap values for each unique pair of participants, such that a larger distance indicates decreased similarity. We then applied the nonparametric Wilcoxon signed-ranks test to the pimfs Wasserstein metric data to assess whether the pimfs components differed in terms of interindividual variability of the pattern of network overlap.

Individual Level: Exploring Functional Dissociations in the Midnight Scan Club Data Set

To further probe sulcal-functional correspondences at the individual level, we leveraged the extensive resting-state fMRI data for the 10 participants from the Midnight Scan Club (MSC; 50% female, aged between 24 and 34 years; Gordon, Laumann, Gilmore, et al., 2017). Briefly, the anatomical T1-w scans and individually derived resting-state fMRI parcellations were acquired from the MSC repository (https://openfmri.org/dataset/ds000224/). Cortical surface reconstructions were generated with FreeSurfer, and the pimfs components were defined, when present, in all 10 participants (20 hemispheres) by E. H. W. and K. S. W. The MSC functional network parcellations were resampled from *fs_LR* 32 k space for each participant onto the fsaverage cortical surface and then to each native surface with Workbench Commands (*wb_command*). The incidence rates of the pimfs components in this smaller sample were similar to what we have observed previously (60% of left and right hemispheres had two components; the pimfs-d was present in 80% of left and right hemispheres, and the pimfs-v was present in 80% of left and right hemispheres). Given the small sample size, we describe the relationship between the pimfs sulcal components and networks qualitatively (Results section and Figure A5).

Group Level: Comparing Co-localization of the Paraintermediate Frontal Sulcus Components with Classic and Modern Group-level Parcellations of the Cerebral Cortex

Finally, we sought to situate the pimfs components with respect to modern and classic cortical parcellations. In the main text, we highlight two parcellations: the group-level HCP 180-region multimodal parcellation (HCP-MMP), derived from topography, architecture, function, and connectivity (Glasser et al., 2016), as well as Brodmann's (1909) cytoarchitectonic parcellation mapped onto the fsavarage surface (i.e., the PALS B12 Brodmann atlas; Van Essen, 2005). We specifically focused on the HCP-MMP because it is based on multiple anatomical and functional metrics and was derived from the sample used in the present study (Glasser et al., 2016). We also focused on Brodmann's cytoarchitectonic parcellation because it is foundational to the field of brain mapping, having been used to identify the location of different functional areas in thousands of studies (Zilles, 2018).

We adopted a similar procedure to the one used for the individually derived parcellations described above. First, we resampled the pimfs components of each participant to the common fsaverage surface, which the HCP-MMP and Brodmann parcellations were also mapped onto (Glasser et al., 2016; Van Essen, 2005). Second, for each participant and hemisphere, we calculated the Dice coefficient to measure the overlap between each sulcal component and the group-level parcellations in the HCP-MMP and Brodmann atlases that comprise LPFC: specifically, eight HCP-MMP regions (IFS-p, IFS-a, p9–46v, 46, 9–46d, a9–46v, p47r, a47r) and six Brodmann's areas (BAs; 45, 46, 47, 9, 10, 11). Third, we ran an rm-ANOVA (factors: Sulcal Component [pimfs-d and pimfs-v] × ROI × Hemisphere [left and right]) to determine if the pimfs-d and

pimfs-v were differentiable from one another based on each parcellation.

We then repeated this pipeline with three additional cortical parcellations. First, we used the modern, functional connectivity-based Brainnetome atlas (Fan et al., 2016; specifically nine LPFC regions: inferior frontal junction, A8vl, A9/46d, A9/46v, IFS, A46, A45r, A10l, and A12/47 l). Second, we used the classic Von Economo and Koskinas cytoarchitecture parcellation (von Economo & Koskinas, 1925)—specifically five LPFC regions: FC, FD, FDdelta, FDT, and FF—which was recently projected to the fsaverage surface by Scholtens and colleagues (2018). Third, we used the classic myeloarchitecture parcellation of the Vogt-Vogt school (Vogt & Vogt, 1919; specifically seven LPFC regions: 48, 49, 52, 53, 54, 58, 59), which was also recently projected to the fsaverage surface by Foit and colleagues (2022). The same format of rm-ANOVA was applied in these cases as well.

Statistics

All statistical tests were implemented in R (v4.0.1; www.r-project.org). Rm-ANOVAs were implemented with the *lme* function and *anova* functions from the *nlme* R and *stats* R packages, respectively. Effect sizes for the rm-ANOVAs are reported with the partial eta-squared (η^2) metric. Relevant post hoc pairwise comparisons on rm-ANOVA effects were computed with the *emmeans* and contrast functions from the emmeans R package (p values adjusted with Tukey's method). The effect size for post hoc pairwise comparisons is reported with Cohen's d (d) metric. Wasserstein distance was calculated with the *wasserstein1d* function from the *transport* R package. The Wilcoxon test was implemented with the *wilcox.test* function from the *stats* R package. If an effect or interaction with a factor (such as hemisphere) is not explicitly reported, it is not significant.

RESULTS

When Present, the Dorsal and Ventral Components of the Pimfs Differ Based on Individual-level Morphological and Architectural Data

As described in the Methods section and in our recent work (Willbrand, Jackson, et al., 2023; Willbrand, Voorhies, et al., 2022), the pimfs components are two variable sulci in the aMFG, identified based on their proximity to the more prominent and superior imfs (Figure 1). The dorsal pimfs is inferior to the horizontal imfs, whereas the ventral pimfs is inferior to the ventral imfs (Figure 1). Both sulci are superior and anterior to the ifs (Figure 1). The pimfs is also variably present across the 72 young adult participants in this sample (see example hemispheres in Figure 1): In a given hemisphere, individuals may have two, one, or zero components. In this sample, the pimfs-d was present in 89% of the left and 88% of the right hemispheres, whereas the pimfs-v was present in 81% of the left and 89% of the right hemispheres (Willbrand, Jackson, et al., 2023). With regard to the number of components present, both pimfs-d and pimfs-v were present in 72% of the left and 78% of the right hemispheres, a single one was present in 25% of the left and 21% of the right hemispheres, and neither was present in 3% of the left and 1% of right hemispheres.

After defining the pimfs components, we tested, based on four metrics, whether they differed morphologically and architecturally from one another and from neighboring sulci (Methods section). Morphologically, we tested sulcal surface area (normalized to hemispheric surface area) and depth (normalized to maximal sulcal depth in a given hemisphere), because these are two of the primary features used to describe sulci (e.g., Li et al., 2022; Miller, Voorhies, et al., 2021; Natu et al., 2021; Lopez-Persem et al., 2019; Madan, 2019; Petrides, 2019; Weiner, 2019; Armstrong et al., 1995; Welker, 1990; Chi et al., 1977; Sanides, 1964). Architecturally, we assessed cortical thickness (in mm) and myelination (T1-w/T2-w ratio; Figure 2A for these values displayed on example hemispheres), as they are additional metrics commonly used to describe and compare sulci (e.g., Willbrand, Ferrer, et al., 2023; Willbrand, Parker, et al., 2022; Yao et al., 2022; Ammons et al., 2021; Miller, Voorhies, et al., 2021; Voorhies et al., 2021; Miller et al., 2020; Natu et al., 2019; Bertoux et al., 2019; Alemán-Gómez et al., 2013; Fornito et al., 2008).

An rm-ANOVA (factors: Sulcal Component [pimfs-d and pimfs-v] × Metric [surface area, depth, cortical thickness, and myelination] × Hemisphere [left and right]) revealed a Sulcal Component × Metric interaction, $F(3, 735) = 5.50$, $\eta^2 = .02$, $p = .001$. Post hoc pairwise comparisons revealed that (i) the pimfs-d was, on average, 15.73% smaller than the pimfs-v ($d = 0.34$, $p = .005$); (ii) there were no differences in sulcal depth ($d = 0.10$, $p = .38$); (iii) the pimfs-d was, on average, 2.48% cortically thicker than the pimfs-v ($d = 0.26$, $p = .020$); and (iv) the pimfs-d was, on average, 0.81% less myelinated than the pimfs-v ($d = 0.30$, $p = .029$; Figure 2B). Removing outliers did not meaningfully impact this interaction or the subsequent post hoc comparisons; in fact, doing so made some of the differences numerically stronger, interaction, $F(3, 714) = 6.67$, $\eta^2 = .03$, $p < .001$; surface area ($d = 0.38$, $p = .001$; pimfs-d 16.36% smaller than pimfs-v on average); depth ($d = 0.10$, $p = .32$); cortical thickness ($d = 0.35$, $p = .015$; pimfs-d 2.92% thicker than pimfs-v on average); and myelination ($d = 0.33$, $p = .010$; pimfs-d 0.81% less myelinated than pimfs-v on average). Furthermore, the surface area, depth, cortical thickness, and myelination of the pimfs-d and pimfs-v did not differ based on the presence/absence of the other component (ps > .31). Both pimfs components were also substantially smaller and shallower—and, in some cases, cortically thicker and less myelinated—than neighboring sulci (Appendix and Figure A1). Altogether, these results indicate that the pimfs-d and pimfs-v are dissociable on the basis of morphology (surface area) and architecture (cortical thickness and myelination) at the level of individual participants.

When Present, the Ventral and Dorsal Components of the Pimfs Are Dissociable Based on Individual-level Functional Parcellations

Classic and recent work implicate the topography of some tertiary sulci in the functional organization of association cortices (Willbrand, Parker, et al., 2022; Miller, D'Esposito, et al., 2021; Miller, Voorhies, et al., 2021; Troiani et al., 2016, 2020; Lopez-Persem et al., 2019; Weiner, 2019; Li et al., 2015; Amiez & Petrides, 2014; Amiez et al., 2013; Sanides, 1964). Particularly relevant to the present study, our prior work indicated that the pMFG tertiary sulci were dissociable based on their relationship to fMRI connectivity networks (Miller, Voorhies, et al., 2021). Therefore, we sought to extend this assessment to the pimfs components in the aMFG.

To this end, we leveraged individual-level resting-state functional connectivity parcellations in the HCP sample (Kong et al., 2019). Importantly, these individual-level parcellations were developed without consideration for cortical folding (and therefore blind to our sulcal labels). For each pimfs component, we calculated the overlap with eight and 17 functional network parcellations via the Dice coefficient (Methods section). Akin to prior work on individual-level functional network variations (Seitzman et al., 2019; Gordon, Laumann, Gilmore, et al., 2017), this procedure generated a functional profile for each pimfs component for each participant that is reflective of whole-brain connectivity patterns (see Figure 3A for an example of this individual-level sulcal-network overlap; see Figure A3 and A4 for all participants).

We first assessed the relationship between the pimfs components and eight broad functional connectivity networks identified at the level of individual participants by Kong and colleagues (2019; auditory, control, default, dorsal attention, somatomotor, temporal-parietal, ventral attention/salience, visual). An rm-ANOVA (factors: Sulcal Component [pimfs-d and pimfs-v] × Network [8 networks] × hemisphere [left and right]) revealed a Sulcal Component × Network interaction, $F(7, 1659) = 55.09$, $\eta^2 = .19$, $p < .001$. Post hoc pairwise comparisons revealed a double dissociation: pimfs-d overlapped more with the ventral attention/salience network ($d = 0.95$, $p < .001$; pimfs-d: mean ± SE = 0.60 ± 0.03, pimfs-v: mean ± SE = 0.27 ± 0.03; Figure 3B), whereas pimfs-v overlapped more with the control network ($d = 0.92$, $p < .001$; pimfs-d: mean ± SE = 0.52 ± 0.03, pimfs-v: mean ± SE = 0.82 ± 0.02; Figure 3B). There was also a Sulcal Component × Network × Hemisphere interaction, $F(7, 1659) = 2.78$, $\eta^2 = .01$, $p = .007$, such that the pimfs-d overlapped more with the control network in the right hemisphere ($d = 0.25$, $p = .004$) and with the ventral attention/salience network in the left hemisphere ($d = 0.22$, $p = .015$), thereby indicating that the dissociation was stronger in the left hemisphere (Figure 3B). In addition, the pattern of overlap between a given component and the networks did not differ based on whether the other component was present (ps > .40).

We then assessed the degree of overlap of the pimfs components with the subnetworks of these aforementioned networks (Control A, Control B, Control C, Ventral Attention/Salience A, Ventral Attention/Salience B; Figure 3A). Once again, an rm-ANOVA (factors: Sulcal Component [pimfs-d and pimfs-v] × Network [17 networks] × hemisphere [left and right]) revealed a Sulcal Component × Network interaction, $F(16, 3792) = 26.93$, $\eta^2 = .10$, $p < .001$. Post hoc pairwise comparisons revealed that the pimfs-d overlapped more with Ventral Attention/Salience B subnetwork ($d = 0.94$, $p < .001$; Figure 3C), whereas the pimfs-v overlapped more with the three control subnetworks: Control A ($d = 0.13$, $p = .022$), Control B ($d = 0.86$, $p < .001$), and Control C ($d = 0.27$, $p < .001$; Figure 3C). It is worth noting that the overlap of pimfs-d with the broad ventral attention/salience network was driven by strong overlap with a single subnetwork, Ventral Attention B (Figures 3C, A3, and A4) at the level of individual participants. By contrast, the overlap of the pimfs-v was more variable across individuals, being split among all three control subnetworks (Figures 3C, A3, and A4). This observation was statistically supported by the finding that pimfs-v had a larger Wasserstein distance ($W = 6.07 \times 10^6$, $p < .001$; pimfs-d: mean ± SE = 0.0311 ± 0.0003, pimfs-v: mean ± SE = 0.0325 ± 0.0003), indicating decreased similarity and therefore greater variability between participants (Methods section). As with the broad functional networks, the relationships between each component and the functional subnetworks did not differ based on whether the other component was present (ps > .37).

To ensure that this differential relationship in sulcal-network overlap was also not limited to the parcellation by Kong and colleagues (2019), we examined the overlap between the pimfs components and individually defined functional parcellations in the MSC data set: an independent sample with individually derived functional parcellations (Gordon, Laumann, Gilmore, et al., 2017). Critically, even when examining this smaller sample ($n = 10$ participants; Methods section), the results are consistent with a functional dissociation between pimfs components. The pimfs-d often served as the border between the fronto-parietal network and cingulo-opercular network as defined by the MSC (examples in Figure A5A). On the other hand, the pimfs-v was often located within the fronto-parietal network in multiple hemispheres (examples in Figure A5B). Altogether, our analyses indicate that the pimfs-d and pimfs-v are functionally dissociable, despite being in close cortical proximity to one another and despite differences in network parcellations and nomenclature across data sets.

Components of the Paraintermediate Frontal Sulcus Can Disappear on Average Surfaces: Implications for Neuroimaging Studies Performing Group Analyses

The variable presence of the pimfs can affect neuroimaging studies aimed at assessing structural-functional

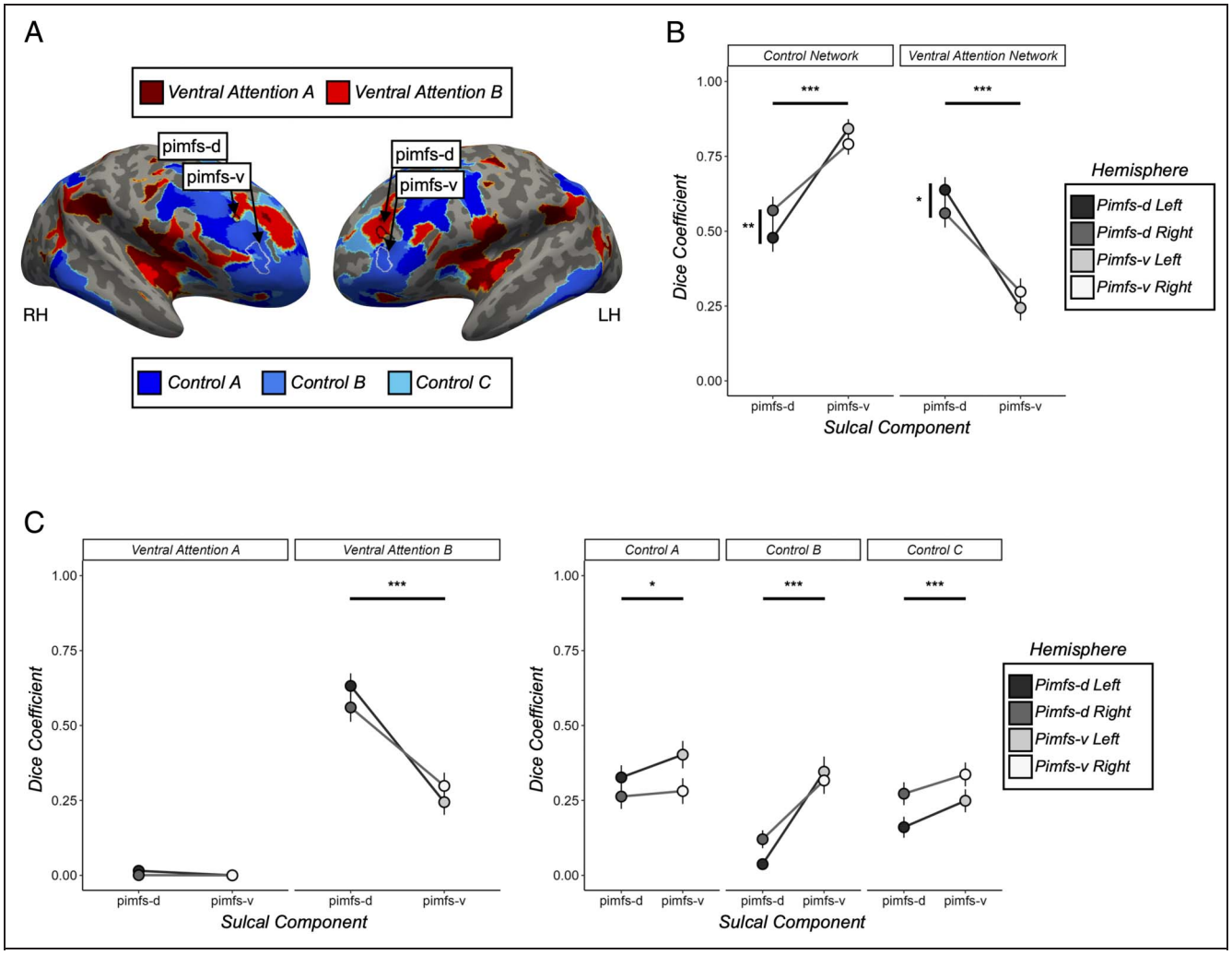

Figure 3. The pimfs-d and pimfs-v are functionally distinct based on functional connectivity parcellations in each individual hemisphere. (A) Example left (LH) and right (RH) hemispheres displaying the relationship between the pimfs components (pimfs-d: black outline; pimfs-v: white outline) and the ventral attention/salience networks (red areas), as well as the control networks (blue areas) as defined by Kong and colleagues (2019). We only visualize these two broad networks/five subnetworks, as they are the only ones prominently overlapping with the pimfs. In addition, although we only show one example individual, these parcellations were conducted in each individual hemisphere for each HCP participant (see Kong et al., 2019, for details). (B) Dice coefficients are plotted as a function of sulcal component (*x* axis; pimfs-d: black, pimfs-v: white), broad networks (facets), and hemisphere (left hemisphere: darker shades; right hemisphere: lighter shades). Large dots and error bars represent mean ± standard error. Horizontal lines and asterisks indicate the significance of the post hoc pairwise comparisons stemming from the Sulcus × Network interaction on Dice coefficient overlap (*$p < .05$, **$p < .01$, ***$p < .001$). Vertical lines and asterisks indicate the significance level of the post hoc pairwise comparisons stemming from the Sulcus × Network × Hemisphere interaction. (C) is the same as (B), but for subnetworks: the ventral attention/salience and control subnetworks. Lines and asterisks indicate the significance level of the post hoc pairwise comparisons stemming from the Sulcus × Network interaction on Dice coefficient overlap. Although there was a Sulcus × Network × Hemisphere for the broad networks, this interaction was not significant with the subnetworks ($p = .19$).

correspondences using group analyses and averaged cortical surface reconstructions. For example, the putative "averaged" pimfs components are visible in the left, but not right, hemisphere of the commonly used fsaverage template (which is made from 39 participants; see https://surfer.nmr.mgh.harvard.edu/fswiki/FsAverage for additional details; Figure 4A). Notably, the fact that two components are visible in the left-hemisphere *fsaverage* template does not mean that the pimfs components are more common in the left hemisphere. Both in this adult sample (Willbrand, Jackson, et al., 2023) and a previous pediatric sample (Willbrand, Voorhies, et al., 2022), the incidence of pimfs-d and pimfs-v do not differ significantly across hemispheres.

Beyond freely available templates such as the *fsaverage* surface, pimfs components can disappear when averaging randomly chosen cortical surfaces from large databases, such as the HCP used in the present study (Glasser et al., 2013). For example, when randomly choosing either 100 or 650 HCP participants, the pimfs components are no longer visible in the left hemisphere (Figure 4A) and probabilistic locations of the pimfs do not clearly align with identifiable structures on averaged surfaces (Figure 4B). This highlights the variability of the pimfs and, more

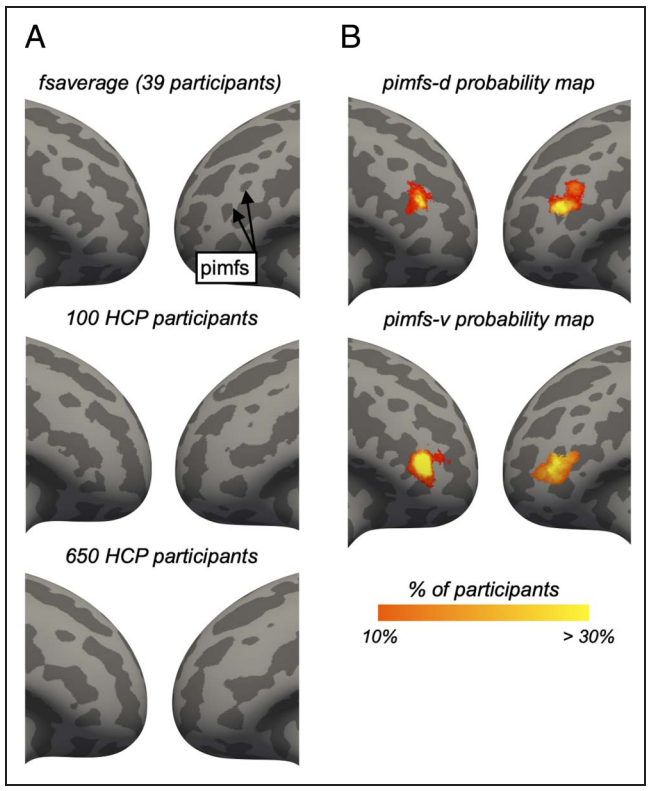

Figure 4. Paraintermediate frontal sulcal components can disappear on average surfaces. (A) The variability of the pimfs in the aMFG can cause them to disappear when individual surfaces are averaged together. Surfaces are focused on LPFC, as in Figure 1. Top to bottom: (i) fsaverage surface (39 participants), (ii) 100 HCP participants, (iii) 650 HCP participants. The disappearance of these sulci on average surfaces, which are often used for group analyses in neuroimaging research, emphasizes the importance of defining these structures on individual hemispheres (Figure 1). (B) Probabilistic maximum probability maps (thresholded at 10% of vertex overlap across participants) of the pimfs-d (top) and pimfs-v (bottom) on the fsaverage surface (from Willbrand, Jackson, et al., 2023), showing that the likely location of the pimfs components do not necessarily align with clearly identifiable structures on average surfaces.

generally, how anatomical variability could affect neuroimaging studies focused on anatomical–functional correspondences, thereby necessitating analyses at the level of individual participants.

Despite this discrepancy between the identification of pimfs components on individual surfaces compared with group templates, there is utility in assessing the location of the pimfs relative to recent and classic parcellations of the cerebral cortex. Such an exercise situates the pimfs in the broader conversation among areas commonly explored in cognitive neuroscience. To do so, we assessed whether the pimfs components also differed in their overlap with a well-cited group-level modern multimodal parcellation (HCP-MMP; Glasser et al., 2016) and a classic microstructural parcellation (Brodmann's classic cytoarchitectonic parcellation; Van Essen, 2005; Brodmann, 1909; Methods section; Figure 5). While we highlight these two modern and classic parcellations, we also consider three additional parcellations at the group level (Brainnetome; Fan et al., 2016, myeloarchitecture; Vogt & Vogt, 1919, and cytoarchitecture; von Economo & Koskinas, 1925; Figure A6).

With regard to the HCP-MMP, the pimfs-d showed similar overlap with Area 46 (mean ± *SE* = 0.46 ± 0.03) and Area a9–46v (mean ± *SE* = 0.40 ± 0.03), whereas the pimfs-v showed the highest overlap with Area a9–46v (mean ± *SE* = 0.68 ± 0.02; Figure 5B). In classic anatomical terms (Cunningham, 1892), these data suggest that the pimfs-d may serve as a limiting sulcus (i.e., a boundary) separating Areas 46 and a9–46v, whereas pimfs-v may serve as an axial sulcus (i.e., co-localizing with) for Area a9–46v (Figure 5B). The possibility that pimfs-d and pimfs-v serve as limiting and axial sulci, respectively, is also suggested by individual-level data from the MSC functional parcellation (Figure A5). On the other hand, overlap with Brodmann's cytoarchitectural parcellation suggests that both pimfs components may be axial sulci for separate BAs. In this parcellation, the pimfs-d overlaps strongly with BA 46 (mean ± *SE* = 0.75 ± 0.03), whereas the pimfs-v overlaps with BA 10 (mean ± *SE* = 0.75 ± 0.03; Figure 5D). Importantly, however, the associations between the pimfs components and Brodmann's cytoarchitectonic parcellation (Figure 5D) are tentative as their identification was observer dependent (Van Essen, 2005; Brodmann, 1909). Therefore, a necessary future direction is to quantify the relationship between the pimfs components (when present) relative to cytoarchitectonic areas that are defined based on modern, observer-independent algorithms in individual hemispheres (Amunts et al., 2020).

DISCUSSION

By applying a multimodal and multiscale approach in individual participants, we demonstrated that the pimfs-d and pimfs-v—two variable sulci in anterior LPFC—are anatomically and functionally dissociable cortical structures (Figure 1). The present study builds on the growing literature examining the relationship between putative tertiary sulci relative to anatomical and functional features of association cortices. In classic anatomical terms (Cunningham, 1892), a sulcus is axial when it is located within a cortical area or limiting when it identifies a boundary between cortical areas. For example, recent and ongoing research findings indicate that the inframarginal sulcus is an example of an axial sulcus in posterior cingulate cortex (Willbrand, Parker, et al., 2022), whereas the midfusiform sulcus is an example of a limiting sulcus identifying boundaries among four cytoarchitectonic areas and multiple large-scale functional maps in ventral temporal cortex (Weiner, 2019).

In addition to the fact that sulci can identify cortical areas or boundaries between areas, individual differences in the morphology of sulci are related to individual differences in cognition, as well as anatomical and functional features of association cortices. For example, in medial

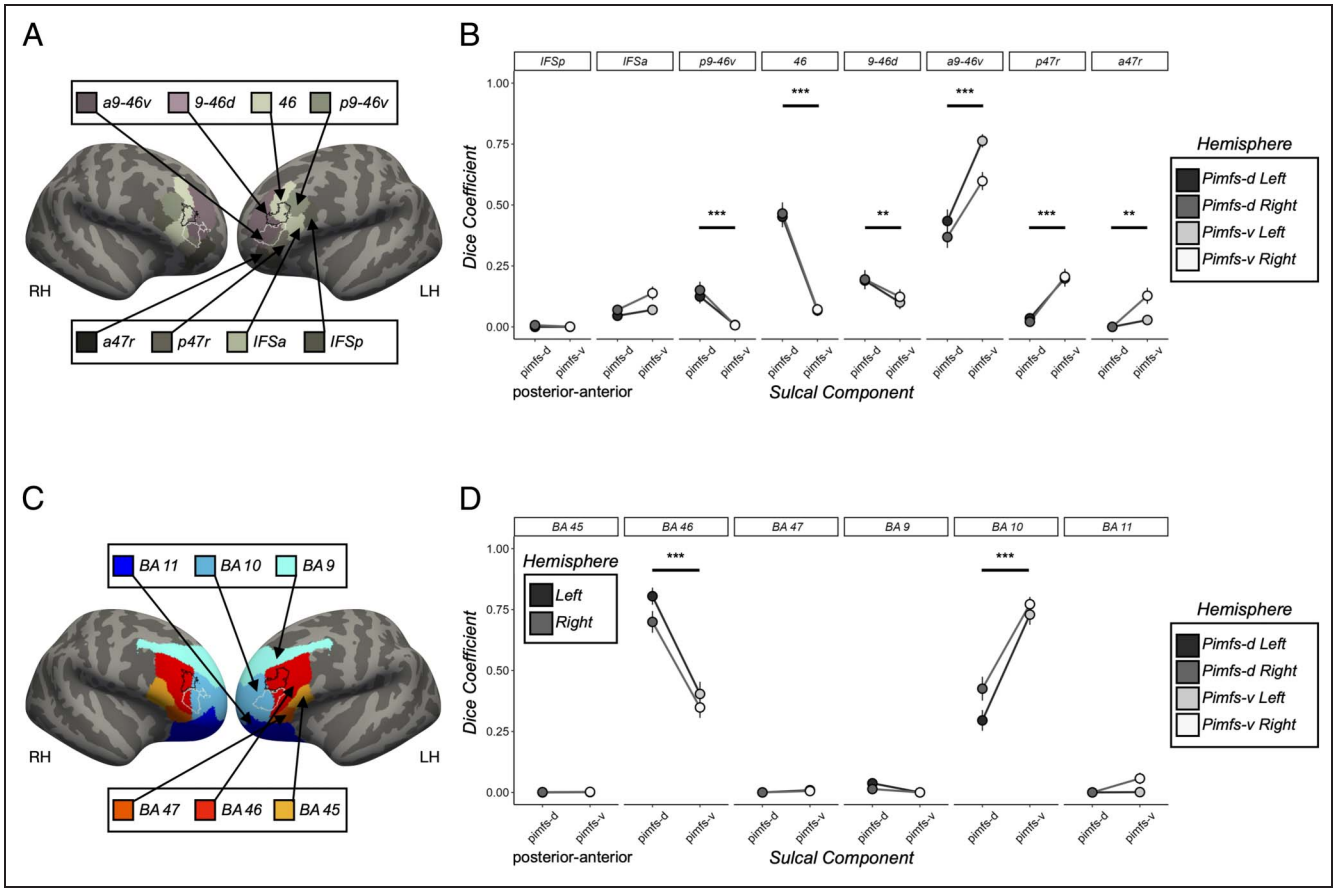

Figure 5. Pimfs components overlap with different regions in modern multimodal and classic cytoarchitectonic group-level cortical parcellations. (A) Left (LH) and right (RH) fsaverage hemispheres displaying the relationship between the probabilistic location of the pimfs components (pimfs-d: black outline; pimfs-v: white outline; from (Willbrand, Jackson, et al., 2023) and eight LPFC regions in the HCP-MMP parcellation (Glasser et al., 2016). (B) Dice coefficient overlap visualized as a function of sulcus (*x* axis; pimfs-d: black, pimfs-v: white), HCP-MMP regions (subplots), and hemisphere (LH: darker shades; RH: lighter shades; see key). Large dots and error bars represent mean ± standard error (*SE*). Horizontal lines and asterisks (***$p < .001$, **$p < .01$) indicate the significant post hoc pairwise comparisons from a Sulcal Component × Region interaction, rm-ANOVA, factors: Sulcal Component (pimfs-d and pimfs-v) × Region × Hemisphere (LH and RH); $F(7, 1701) = 55.64$, $\eta^2 = .19$, $p < .001$. This interaction was driven by the pimfs-d overlapping more with areas p9–46v ($d = 0.72$, $p < .001$), 9–46d ($d = 0.30$, $p = .003$), and 46 ($d = 1.40$, $p < .001$) and the pimfs-v overlapping more with Areas a9–46v ($d = 0.86$, $p < .001$), p47r ($d = 0.89$, $p < .001$), and a47r ($d = 0.55$, $p = .005$). (C) is the same as (A), except for the six LPFC regions in Brodmann's cytoarchitectonic parcellation (Van Essen, 2005; Brodmann, 1909). (D) is the same format as (B), but with Brodmann's cytoarchitectonic parcellation. Again, there was a Sulcal Component × Region interaction, $F(5, 1215) = 93.19$, $\eta^2 = .28$, $p < .001$. This interaction was driven by the pimfs-d overlapping more with BA 46 ($d = 1.12$, $p < .001$; pimfs-d: mean ± *SE* = 0.75 ± 0.03, pimfs-v: mean ± *SE* = 0.38 ± 0.03) and pimfs-v overlapping more with BA 10 ($d = 1.20$, $p < .001$; pimfs-d: mean ± *SE* = 0.36 ± 0.03, pimfs-v: mean ± *SE* = 0.75 ± 0.03). Additional modern and classic cortical parcellations are shown in Figure A6.

pFC, the presence/absence of the paracingulate sulcus affects the location of cytoarchitectonic boundaries in humans and chimpanzees (Amiez et al., 2021) and the location of task-based activation (Amiez & Petrides, 2014; Amiez et al., 2013; Crosson et al., 1999), with network (Lopez-Persem et al., 2019) and cognitive implications in neurotypical (Amiez, Wilson, & Procyk, 2018; Borst et al., 2014; Fornito et al., 2004) and clinical (Rollins et al., 2020; Garrison et al., 2015; Fornito et al., 2006) populations. Below, we discuss how the combination of the present and previous findings support the idea that putative tertiary sulci serve as "personalized coordinates" related to variability in regional anatomical and functional organization in association cortices, as well as cognition. We then discuss the limitations and future directions of this work.

Tertiary Sulci as "Personalized Coordinates" Related to Variability in Regional Anatomical and Functional Organization in Association Cortices, as well as Individual Differences in Cognition

The present study shows that pimfs-d and pimfs-v are anatomically and functionally dissociable structures, thereby justifying the use of distinct anatomical labels for these sulci in current and future research. Recently, we (Miller, D'Esposito, et al., 2021) proposed that putative tertiary sulci are situated in a unique position: Although they are

the smallest and shallowest sulci in a cortical expanse, these structures can offer insights across spatial scales, modalities, and species in association cortices, which have expanded the most throughout evolution and are linked to human-specific aspects of cognition. As these sulci can disappear on average cortical surfaces, we further proposed that the location of tertiary sulci within each individual participant serves as a coordinate system specific to that individual on which functions may be further mapped. That is, the identification of these sulci in an individual hemisphere can be neuroanatomically more accurate than coordinates on a standardized brain. For example, consider LPFC structures that are not present in every hemisphere—namely, the pimfs—or LPFC structures that are present (to our knowledge) in every hemisphere, such as components of the posterior middle frontal sulcus (Miller, Voorhies, et al., 2021). In both cases, crosshairs on a standardized brain may be centered on a gyrus when in actuality, the pinpointed location in that participant's hemisphere is located within either the pimfs or one of the posterior middle frontal sulcus components, each of which can disappear on average cortical surfaces. To guide accurate definitions of these sulci by researchers in the broad field of cognitive neuroscience, we have shared probabilistic locations of the pimfs (Figure 4B) with this article, as well as tools to help further semi-automate sulcal definitions in our previous work (Willbrand, Parker, et al., 2022; Lyu et al., 2021).

These probabilistic definitions could help guide a potential relationship between the pimfs components and functional regions beyond those explored here, as well as identify novel hemispheric sulcal-functional correspondences. For example, our previous work indicated that the presence of the left pimfs-v is associated with 21–34% better scores on a test of abstract reasoning in pediatric and adult samples (Willbrand, Jackson, et al., 2023; Willbrand, Voorhies, et al., 2022). Converging with these findings, areal definitions at the group level that overlap the most with the probabilistic definition of the pimfs-v have been implicated in reasoning: (i) Glasser and colleagues (2016) heavily weighted the boundaries of Area a9–46 based on activation during a relational reasoning task and (ii) the lateral aspect of BA 10 or BA 10/46, which also overlaps with the probabilistic definition of pimfs-v (Figure 5C), is routinely activated on a variety of reasoning tasks (Holyoak & Monti, 2021; Westphal et al., 2019; Westphal, Reggente, Ito, & Rissman, 2016; Urbanski et al., 2016; Vendetti & Bunge, 2014; Wendelken, Nakhabenko, Donohue, Carter, & Bunge, 2008; Smith, Keramatian, & Christoff, 2007; Ramnani & Owen, 2004; Christoff & Gabrieli, 2000; Koechlin, Basso, Pietrini, Panzer, & Grafman, 1999)—especially in the left hemisphere (Assem, Glasser, Van Essen, & Duncan, 2020; Hartogsveld et al., 2018; Wendelken et al., 2017; Hobeika, Diard-Detoeuf, Garcin, Levy, & Volle, 2016; Urbanski et al., 2016; Green, Kraemer, Fugelsang, Gray, & Dunbar, 2010; Bunge, Helskog, & Wendelken, 2009; Green, Fugelsang, Kraemer, Shamosh, & Dunbar, 2006; Christoff et al., 2001). This correspondence suggests that pimfs-v may lie within or adjacent to an area of LPFC functionally related to reasoning. In addition, future work should assess whether the incidence of this sulcal component relates to neural activation during reasoning tasks and whether this mediates the behavioral difference seen between individuals who do or do not possess a left pimfs-v component.

Alongside prior work (Willbrand, Parker, et al., 2022; Miller, D'Esposito, et al., 2021; Miller, Voorhies, et al., 2021; Troiani et al., 2016, 2020; Lopez-Persem et al., 2019; Weiner, 2019; Li et al., 2015), the present results suggest that future individual-level parcellations could benefit from incorporating sulcal anatomy when delineating cortical regions—especially within human LPFC, which has been referred to as a "hotspot of individual variability" (Glasser et al., 2016) and has been reported by multiple groups to be an area with extensive individual differences in functional organization (e.g., see Dworetsky et al., 2021; Kong et al., 2021; Li et al., 2019; Seitzman et al., 2019; Gordon, Laumann, Adeyemo, et al., 2017).

Limitations and Future Directions

Although the present work contained a relatively large sample of sulci for detailed analyses at the level of individual participants (249 pimfs definitions, which were informed by the location of surrounding LPFC sulci, resulting in 2985 sulci defined), the primary limitation was the sample size (72 participants; 144 hemispheres). The sample sizes of studies that involve manually defining sulci in individual participants are limited by the time investment and anatomical expertise required to label them (e.g., Willbrand, Parker, et al., 2022; Willbrand, Voorhies, et al., 2022; Yao et al., 2022; Hopkins et al., 2021; Miller, Voorhies, et al., 2021; Voorhies et al., 2021; Nakamura et al., 2020; Amiez et al., 2006, 2018, 2019; Lopez-Persem et al., 2019; Borst et al., 2016; Zlatkina et al., 2016; Garrison et al., 2015; Cachia et al., 2014; Weiner et al., 2014). With the advent of improved methods to automatically define sulci (e.g., Willbrand, Parker, et al., 2022; Lyu et al., 2021; Borne et al., 2020), such sulcal-based studies can begin to increase their scope and scale. However, these methods are still developing, given the large—and still growing—number of sulci identifiable in the human (and nonhuman hominoid) cerebral cortex and the uniqueness of sulcal patterning across individuals. Therefore, for the time being, automatic labeling methods must be used in tandem with manual labeling to further delineate the complex sulcal patterning in a given hemisphere.

The present findings and our prior work demonstrate the feasibility of applying this multimodal approach for dissociating sulci from one another and also determining the relevance of these structures across association cortices (Willbrand, Parker, et al., 2022; Miller, Voorhies, et al., 2021). Future work should adopt these and additional methodologies in other regions and samples to determine

the generalizability of these relationships and explore new questions. For example, although sulci appear in gestation (Chi et al., 1977), sulcal morphology does change during child development (Willbrand, Ferrer, et al., 2023; Im, 2021; Im & Grant, 2019; Vandekar et al., 2015; Klein et al., 2014; Meng, Li, Lin, Gilmore, & Shen, 2014; Alemán-Gómez et al., 2013; Raznahan et al., 2011). Thus, the differences in thickness, myelination, and surface area of the pimfs components may relate to underlying differential rates of development. In addition, although the pimfs components differ in a proxy measure of myelination (T1-w/T2-w ratio), it is unknown if differences in white matter projections could explain or contribute to differences in functional connectivity profiles of the pimfs components. Exploring these possibilities could provide insight into how LPFC hierarchies develop on a microscale. Furthermore, an additional open question is: Are the pimfs components morphologically, anatomically, and functionally distinct at birth, or do they differentiate during infant/child development? These anatomical and functional relationships may also differ as a function of psychiatric or neurological conditions that have roots in prenatal development, when sulci first form (Cachia et al., 2021; Chi et al., 1977). Finally, given the variability of the pimfs and its unique location in LPFC at the convergence between dorsal-ventral and rostral-caudal axes in LPFC, these sulci may serve as a convergence zone for anatomical and functional gradients in LPFC (Miller, D'Esposito, et al., 2021; Miller, Voorhies, et al., 2021; Nee & D'Esposito, 2016; Badre & D'Esposito, 2009).

In conclusion, the present study indicates that individual differences in sulcal variability are related to individual differences in morphological, architectural, and functional features of LPFC. In addition, that putative tertiary sulci may be useful as "personalized coordinates" in a given hemisphere (Miller, D'Esposito, et al., 2021) in "precision neuroimaging" studies (Gratton, Nelson, & Gordon, 2022), with the overarching goal of improving the understanding of neuroanatomical–functional relationships at the level of individual participants, as well as how that relationship contributes to individual differences in cognition.

APPENDIX

The Pimfs Components Differ Anatomically from Surrounding aLPFC Sulci

We also sought to compare the morphological and architectural characteristics of the pimfs components to the surrounding prominent sulci (Methods section; Figure 1). We first compared the pimfs-d to the two surrounding sulci—imfs-h and ifs (Figure 1)—with a rm-ANOVA (factors of Sulcus [pimfs-d, imfs-h, and ifs] × Metric [surface area, depth, cortical thickness, and myelination] × Hemisphere [left and right]). This analysis revealed a Sulcal Component × Metric interaction, $F(6, 1221) = 110.59$, $\eta^2 = .35$, $p < .001$. Post hoc pairwise comparisons revealed that (i) the pimfs-d was, on average, 81.56% smaller than the ifs ($d = 3.55$, $p < .001$) and 66.62% smaller than the imfs-h ($d = 2.74$, $p < .001$); (ii) the pimfs-d was, on average, 78.16% shallower than the

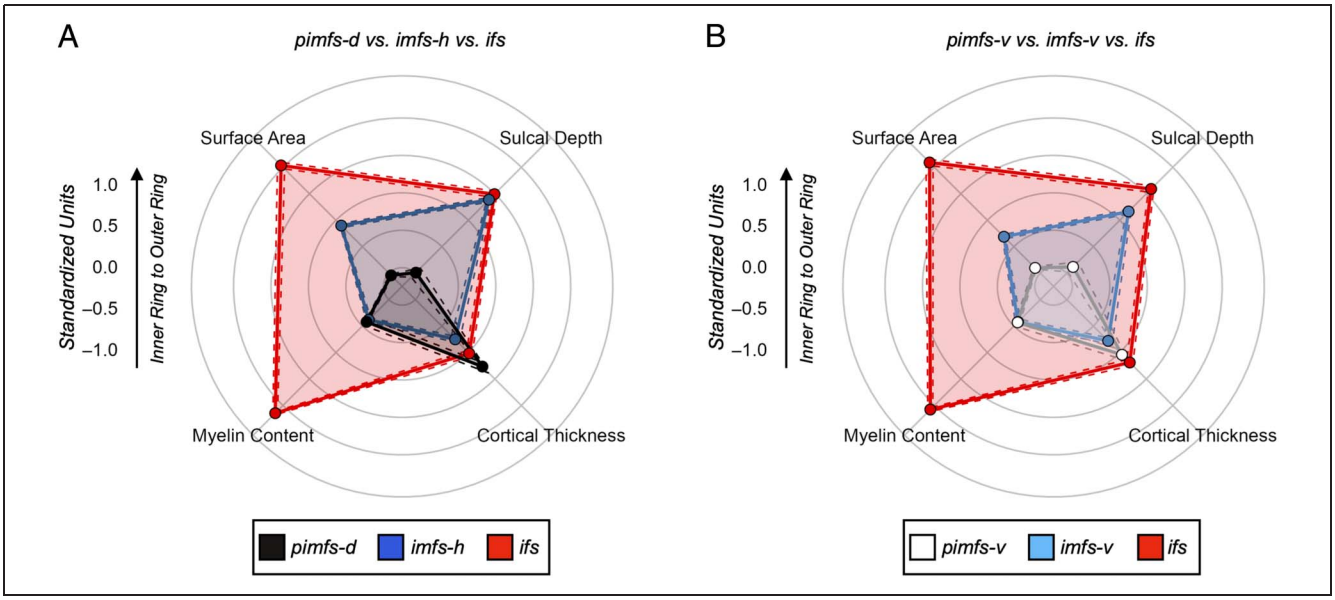

Figure A1. The pimfs components differ in morphology and architecture from the surrounding aLPFC sulci. (A) Polar plots in the same format as in Figure 2, but comparing the morphological (top) and architectural (bottom) features of the pimfs-d to the two surrounding prominent sulci: the ifs and imfs-h (Figure 1). (B) is the same format as in Figure 2, but comparing the pimfs-v to the two surrounding prominent sulci: the ifs and imfs-v (Figure 1).

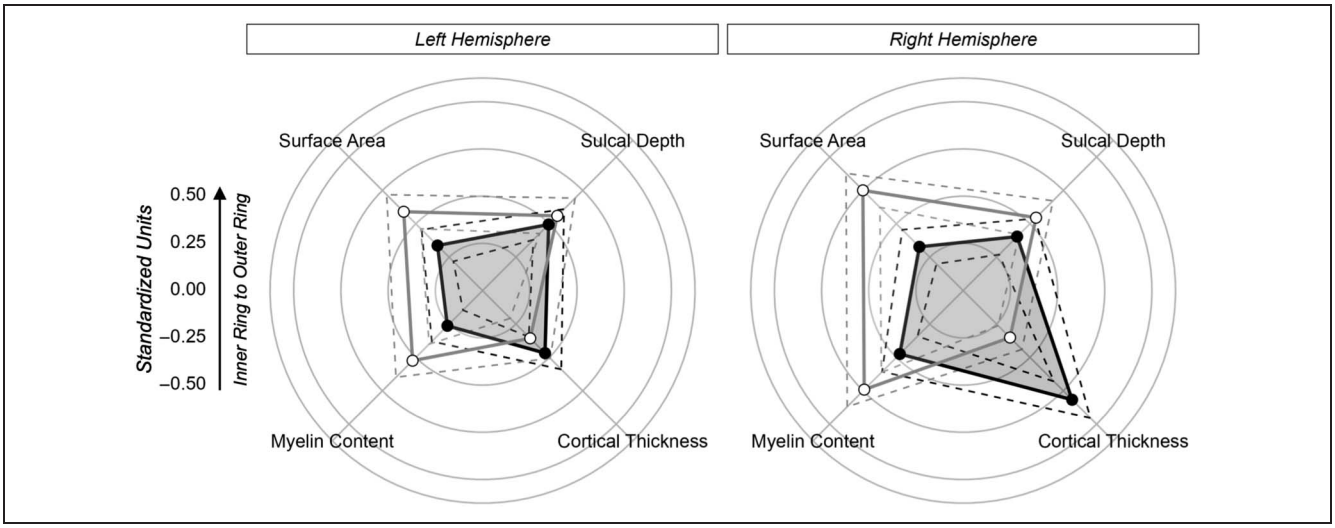

Figure A2. Morphological and architectural features of the pimfs components separately in each hemisphere. Polar plot in the same format as in Figure 2, but for the morphological (top) and architectural (bottom) features of the pimfs components in the left (left facet) and right (right facet) hemispheres separately. As in Figure A1, pimfs-d is shown in black and pimfs-v is shown in white/gray.

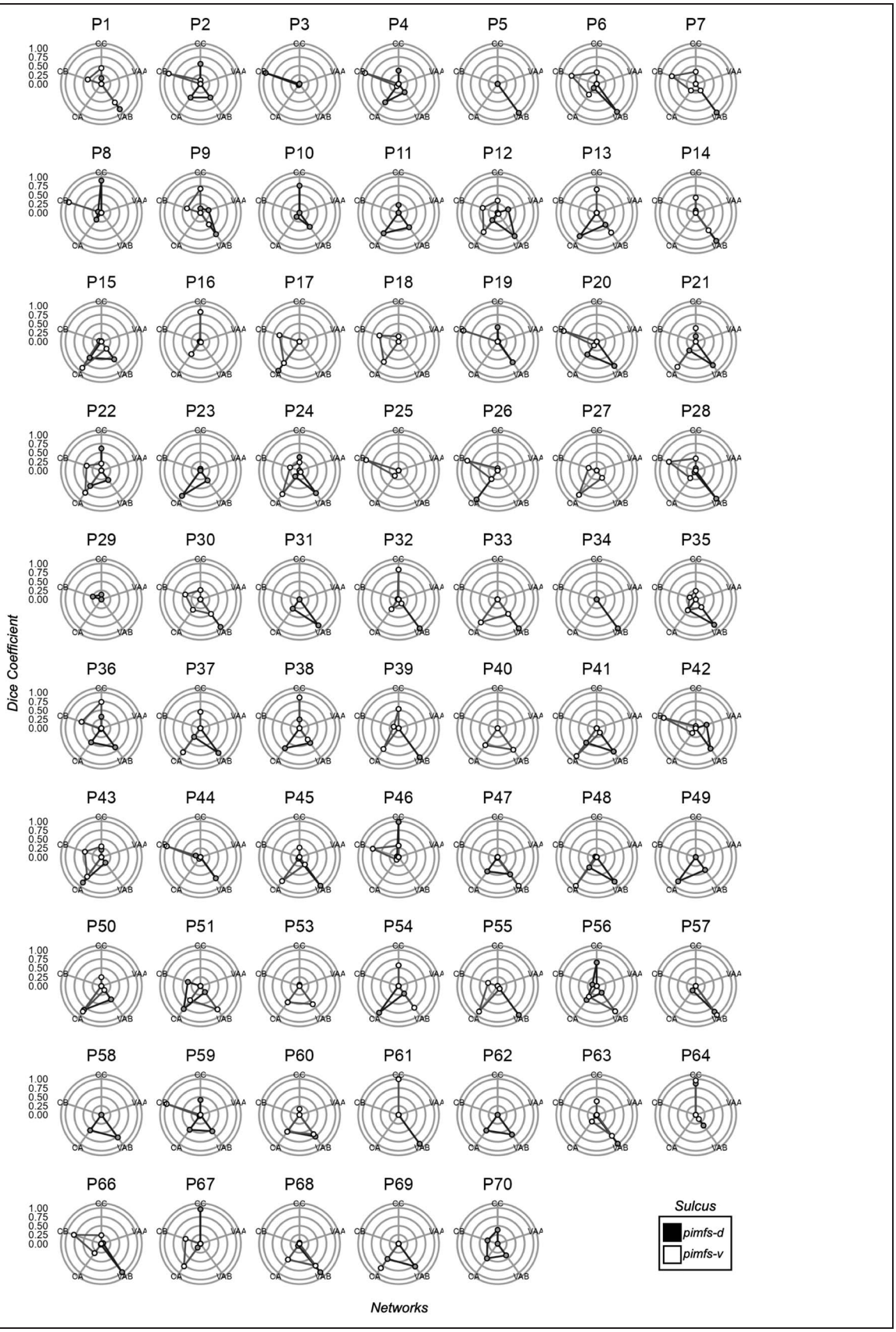

Figure A3. Overlap between the pimfs components and functional parcellations in individual left hemispheres. Polar plots showing the overlap of the pimfs-d and pimfs-v with the control (C) and ventral attention (VA) subnetworks in the left hemisphere of all participants with at least one pimfs component (n = 68). The closer to the periphery of the circle, the higher the Dice coefficient (numbers on the left correspond to the Dice coefficient value at each concentric circle).

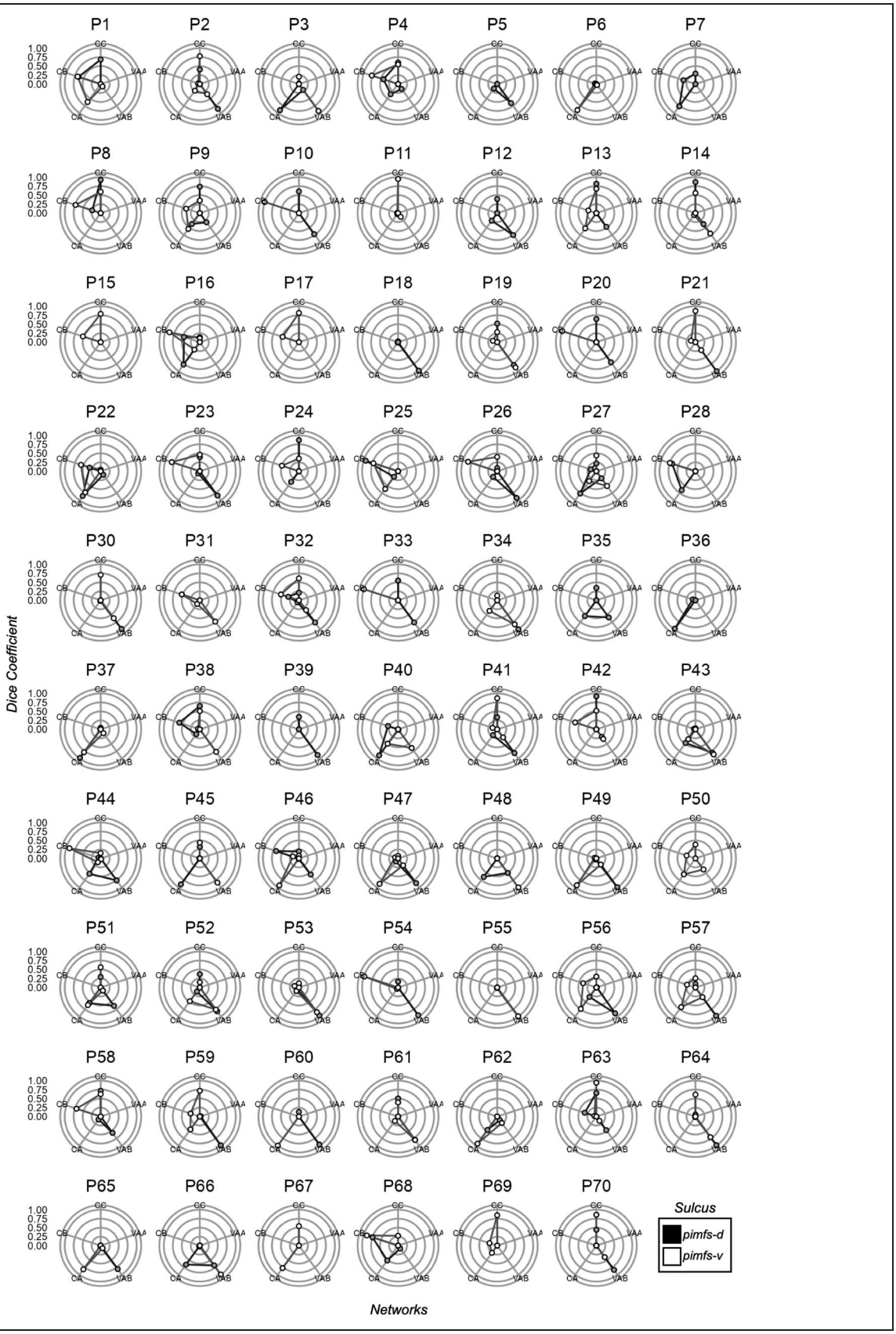

Figure A4. Overlap between the pimfs components and functional parcellations in individual right hemispheres. Polar plots showing the overlap of the pimfs-d and pimfs-v with the control (C) and ventral attention (VA) subnetworks in the right hemisphere of all participants with at least one pimfs component (n = 69). The closer to the periphery of the circle, the higher the Dice coefficient (numbers on the left correspond to the Dice coefficient value at each concentric circle).

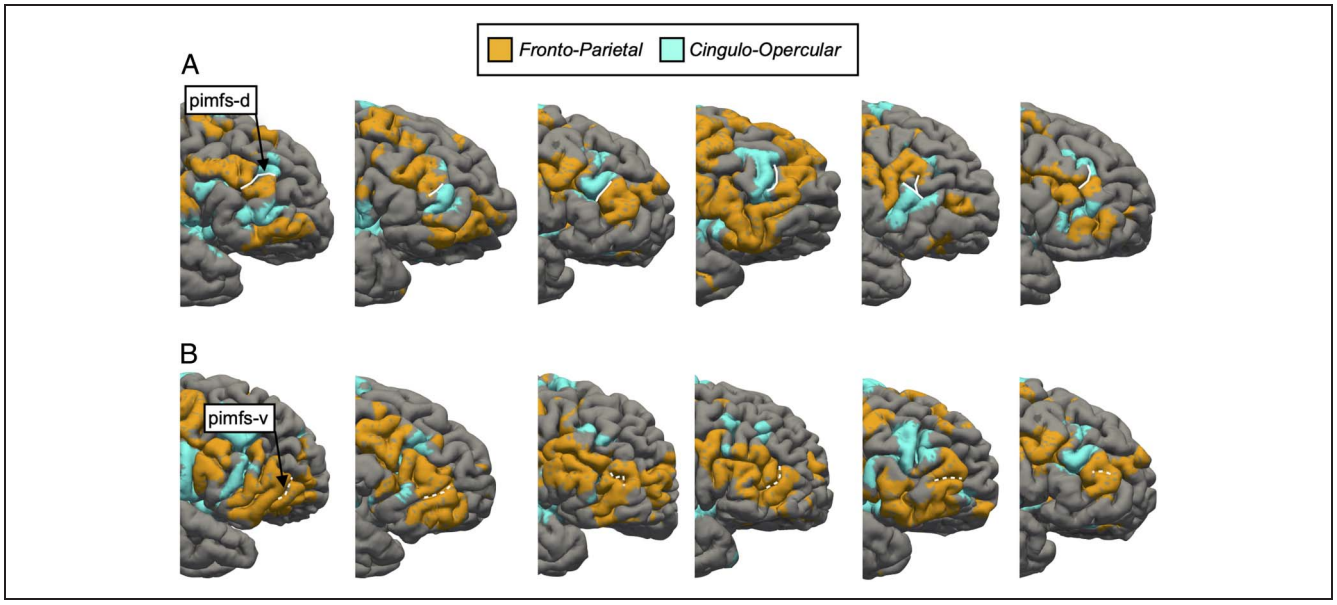

Figure A5. The pimfs components in relation to an additional functional parcellation in individual participants. (A) Pial cortical hemispheres from example MSC participants (n = 10, 20 hemispheres) showing that the pimfs-d (solid white line) often identifies a transition between what is defined as regions of the fronto-parietal (orange) and cingulo-opercular (cyan) networks as defined by Gordon, Laumann, Gilmore, and colleagues (2017). Specifically, the pimfs-d identifies a transition in 13 of the 16 hemispheres in which this component was present. Six example hemispheres are shown and are oriented such that all hemispheres face in the same direction (the specific hemisphere specified in bottom right of each hemisphere) and are zoomed in on the LPFC as in Figure 1. In the remaining three hemispheres, the pimfs-d identified the boundary between the fronto-parietal and other networks: salience and/or dorsal attention. (B) is the same format as (A), but for six example participants showing that the pimfs-v (dashed white line) is often located within the fronto-parietal network as defined by Gordon, Laumann, Gilmore, and colleagues (2017). Specifically, the pimfs-v falls within the fronto-parietal network in 10 of the 16 hemispheres in which this component was identified. In the other six hemispheres, the pimfs-v was located within other networks (cingulo-opercular: 3/16, context: 1/16, undefined expanse: 2/16).

ifs (d = 1.83, p < .001) and 76.88% shallower than the imfs-h (d = 1.70, p < .001); (iii) the pimfs-d was, on average, 1.64% cortically thicker than the ifs (d = 0.22, p < .008) and 3.77% thicker than the imfs-h (d = 0.45, p < .001); and (iv) the pimfs-d was, on average, 6.15% less myelinated than the ifs (d = 2.72, p < .001), but not significantly different in myelination to the imfs-h (p = .85; Figure A1A). Thus, the pimfs-d differed anatomically from its neighbors on all four metrics—most notably in terms of surface area and depth.

We then compared the pimfs-v to the two surrounding sulci, imfs-v and ifs (Figure 1), with a rm-ANOVA (factors of Sulcus [pimfs-d, imfs-h, and ifs] × Metric [surface area, depth, cortical thickness, and myelination] × Hemisphere [left and right]). This analysis revealed a Sulcal Component × Metric interaction, $F(6, 1206)$ = 59.84, η^2 = .23, p < .001. Post hoc pairwise comparisons revealed that (i) the pimfs-v was, on average, 78.11% smaller than the ifs (d = 3.39, p < .001) and 51.28% smaller than the imfs-v (d = 1.61, p < .001); (ii) the pimfs-v was, on average, 72.95% shallower than the ifs (d = 1.68, p < .001) and 65.60% shallower than the imfs-v (d = 1.20, p < .001); (iii) the pimfs-v was, on average, 1.68% cortically thicker than the imfs-v (d = 0.22, p = .015), but not different from the ifs (p = .22); and (iv) the pimfs-v was, on average, 5.38% less myelinated than the ifs (d = 2.39, p < .001), but not significantly different in myelination to the imfs-v (p = .99; Figure A1B). Thus, as with the pimfs-d, the pimfs-v differed anatomically from its neighbors on multiple metrics—again most notably in terms of surface area and depth.

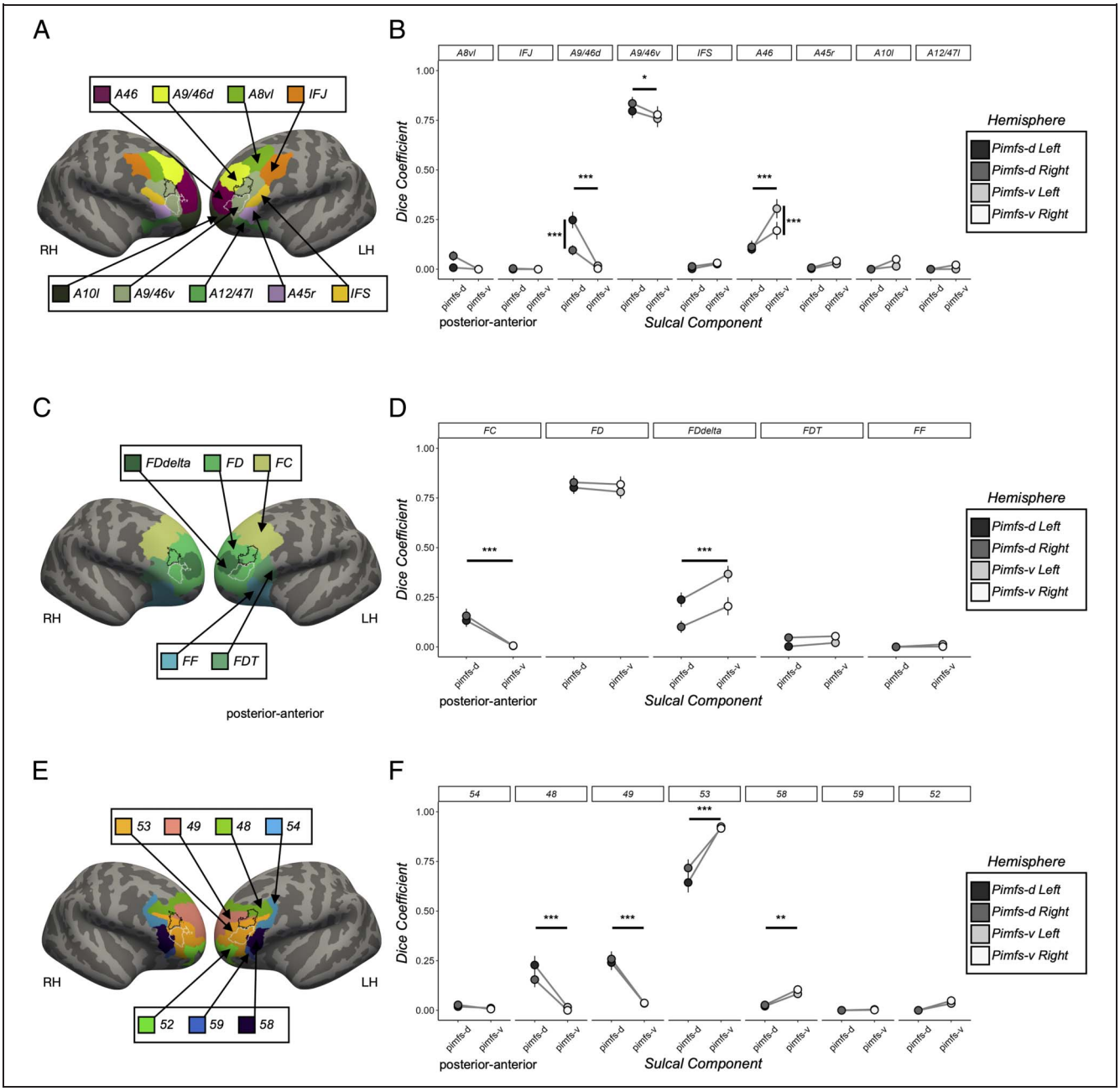

Figure A6. Pimfs components in relation to different areas in additional cortical parcellations. (A) Left (LH) and right (RH) hemisphere *fsaverage* surfaces displaying the relationship between the probabilistic location of the pimfs components (pimfs-d: black outline; pimfs-v: white outline; from [Willbrand, Jackson, et al., 2023] and nine LPFC regions in the Brainnetome resting-state functional connectivity-based parcellation [Fan et al., 2016]). (B) Dice coefficient overlap visualized as a function of sulcus (*x* axis; pimfs-d: black, pimfs-v: white), Brainnetome regions (subplots), and hemisphere (LH: darker shades; RH: lighter shades; see key). Large dots and error bars represent mean ± standard error (*SE*). Horizontal lines and asterisks (***$p < .001$, **$p < .01$, *$p < .05$) indicate the significant post hoc pairwise comparisons from the Sulcal Component × Region interaction, rm-ANOVA: factors: Sulcal Component (pimfs-d and pimfs-v) × Region × Hemisphere (LH and RH); $F(8, 1944) = 14.49$, $\eta^2 = .06$, $p < .0001$. This interaction was driven by the pimfs-d overlapping more with areas A8vl, A9/46d, and A9/46v (ds > 0.15, ps < .028) and the pimfs-v overlapping more with Area 46 ($d = 0.47$, $p < .001$). Vertical lines and asterisks indicate the significant post hoc pairwise comparisons from the Sulcal Component × Region × Hemisphere interaction, $F(8, 1944) = 2.76$, $\eta^2 = .01$, $p < .005$. (C) is the same format as A, except for the five LPFC regions in the cytoarchitectonic parcellation from Von Economo and Koskinas (Scholtens et al., 2018; von Economo & Koskinas, 1925). (D) is the same format as B, but with Von Economo and Koskinas' cytoarchitectonic parcellation. Again, there was a Sulcal Component × Region interaction, $F(4, 972) = 11.88$, $\eta^2 = .05$, $p < .001$. This interaction was driven by the pimfs-d overlapping more with area FC ($d = 0.73$, $p < .001$) and the pimfs-v overlapping more with area FDdelta ($d = 0.36$, $p < .001$). (E) is the same as (A), except for the seven LPFC regions in Vogt and Vogt's myeloarchitectonic parcellation (Foit et al., 2022; Vogt & Vogt, 1919). (F) is the same format as (B), but with Vogt and Vogt's myeloarchitectonic parcellation. Again, there was a Sulcal Component × Region interaction, $F(6, 1458) = 45.42$, $\eta^2 = .06$, $p < .001$. This interaction was driven by the pimfs-d overlapping more with Areas 48 and 49 (ds > 0.30, ps < .001) and the pimfs-v overlapping more with Areas 53 and 58 (ds > 0.52, ps < .003).

Acknowledgments

We thank Jacob Miller, Willa Voorhies, Jewelia Yao, Samantha Jackson, and Szeshuen Chen for their prior assistance in defining LPFC sulci. We also thank Jacob Miller for helping to develop the analysis pipelines implemented in the present work. We also thank the HCP researchers for participant recruitment and data collection and sharing, as well as the participants who took part in the study.

Reprint requests should be sent to Kevin S. Weiner, Department of Psychology, University of California Berkeley, 2121 Berkeley Way West, Berkeley CA 94720, United States, or via e-mail: kweiner@berkeley.edu.

Data Availability Statement

The processed data required to perform all statistical analyses and reproduce all figures used for this project will be made freely available on GitHub upon publication (https://github.com/cnl-berkeley/stable_projects). The analysis pipelines used for this project are also freely available on Open Science Framework (https://osf.io/7fwqk/). Anonymized neuroimaging data for the HCP participants were downloaded from and are available at ConnectomeDB (db.humanconnectome.org). Requests for any additional information should be directed to the corresponding authors: Silvia Bunge (sbunge@berkley.edu) and/or Kevin Weiner (kweiner@berkeley.edu).

Author Contributions

Ethan H. Willbrand: Conceptualization; Data curation; Formal analysis; Investigation; Methodology; Project administration; Visualization; Writing—Original draft; Writing—Review & editing. Silvia A. Bunge: Conceptualization; Funding acquisition; Supervision; Visualization; Writing—Original draft; Writing—Review & editing. Kevin S. Weiner: Conceptualization; Data curation; Formal analysis; Funding acquisition; Investigation; Methodology; Supervision; Visualization; Writing—Original draft; Writing—Review & editing.

Funding Information

This research was supported by NICHD (https://dx.doi.org/10.13039/100009633), R21HD100858 (PIs Weiner and Bunge) and National Science Foundation (NSF; https://dx.doi.org/10.13039/100000001), CAREER Award 2042251 (PI Weiner). The neuroimaging data were provided by the HCP, WU-Minn Consortium (PIs David Van Essen and Kamil Ugurbil; NIH grant 1 U54-MH-091657) funded by the 16 NIH Institutes and Centers that support the NIH Blueprint for Neuroscience Research, and the McDonnell Center for Systems Neuroscience at Washington University.

Diversity in Citation Practices

Retrospective analysis of the citations in every article published in this journal from 2010 to 2021 reveals a persistent pattern of gender imbalance: Although the proportions of authorship teams (categorized by estimated gender identification of first author/last author) publishing in the *Journal of Cognitive Neuroscience* (*JoCN*) during this period were M(an)/M = .407, W(oman)/M = .32, M/W = .115, and W/W = .159, the comparable proportions for the articles that these authorship teams cited were M/M = .549, W/M = .257, M/W = .109, and W/W = .085 (Postle and Fulvio, *JoCN*, 34:1, pp. 1–3). Consequently, *JoCN* encourages all authors to consider gender balance explicitly when selecting which articles to cite and gives them the opportunity to report their article's gender citation balance. The authors of this article report its proportions of citations by gender category to be: M/M = .548; W/M = .237; M/W = .129; W/W = .086.

REFERENCES

Alemán-Gómez, Y., Janssen, J., Schnack, H., Balaban, E., Pina-Camacho, L., Alfaro-Almagro, F., et al. (2013). The human cerebral cortex flattens during adolescence. *Journal of Neuroscience*, *33*, 15004–15010. https://doi.org/10.1523/JNEUROSCI.1459-13.2013, PubMed: 24048830

Amiez, C., Kostopoulos, P., Champod, A.-S., & Petrides, M. (2006). Local morphology predicts functional organization of the dorsal premotor region in the human brain. *Journal of Neuroscience*, *26*, 2724–2731. https://doi.org/10.1523/JNEUROSCI.4739-05.2006, PubMed: 16525051

Amiez, C., Neveu, R., Warrot, D., Petrides, M., Knoblauch, K., & Procyk, E. (2013). The location of feedback-related activity in the midcingulate cortex is predicted by local morphology. *Journal of Neuroscience*, *33*, 2217–2228. https://doi.org/10.1523/JNEUROSCI.2779-12.2013, PubMed: 23365257

Amiez, C., & Petrides, M. (2014). Neuroimaging evidence of the anatomo-functional organization of the human cingulate motor areas. *Cerebral Cortex*, *24*, 563–578. https://doi.org/10.1093/cercor/bhs329, PubMed: 23131805

Amiez, C., Sallet, J., Hopkins, W. D., Meguerditchian, A., Hadj-Bouziane, F., Ben Hamed, S., et al. (2019). Sulcal organization in the medial frontal cortex provides insights into primate brain evolution. *Nature Communications*, *10*, 3437. https://doi.org/10.1038/s41467-019-11347-x, PubMed: 31366944

Amiez, C., Sallet, J., Novek, J., Hadj-Bouziane, F., Giacometti, C., Andersson, J., et al. (2021). Chimpanzee histology and functional brain imaging show that the paracingulate sulcus is not human-specific. *Communications Biology*, *4*, 54. https://doi.org/10.1038/s42003-020-01571-3, PubMed: 33420330

Amiez, C., Wilson, C. R. E., & Procyk, E. (2018). Variations of cingulate sulcal organization and link with cognitive performance. *Scientific Reports*, *8*, 13988. https://doi.org/10.1038/s41598-018-32088-9, PubMed: 30228357

Ammons, C. J., Winslett, M.-E., Bice, J., Patel, P., May, K. E., & Kana, R. K. (2021). The mid-fusiform sulcus in autism spectrum disorder: Establishing a novel anatomical landmark related to face processing. *Autism Research*, *14*, 53–64. https://doi.org/10.1002/aur.2425, PubMed: 33174665

Amunts, K., Mohlberg, H., Bludau, S., & Zilles, K. (2020). Julich-brain: A 3D probabilistic atlas of the human brain's

cytoarchitecture. *Science*, *369*, 988–992. https://doi.org/10.1126/science.abb4588, PubMed: 32732281
Amunts, K., & Zilles, K. (2015). Architectonic mapping of the human brain beyond Brodmann. *Neuron*, *88*, 1086–1107. https://doi.org/10.1016/j.neuron.2015.12.001, PubMed: 26687219
Armstrong, E., Schleicher, A., Omran, H., Curtis, M., & Zilles, K. (1995). The ontogeny of human gyrification. *Cerebral Cortex*, *5*, 56–63. https://doi.org/10.1093/cercor/5.1.56
Assem, M., Glasser, M. F., Van Essen, D. C., & Duncan, J. (2020). A domain-general cognitive core defined in multimodally parcellated human cortex. *Cerebral Cortex*, *30*, 4361–4380. https://doi.org/10.1093/cercor/bhaa023, PubMed: 32244253
Badre, D., & D'Esposito, M. (2009). Is the rostro-caudal axis of the frontal lobe hierarchical? *Nature Reviews Neuroscience*, *10*, 659–669. https://doi.org/10.1038/nrn2667, PubMed: 19672274
Bertoux, M., Lagarde, J., Corlier, F., Hamelin, L., Mangin, J.-F., Colliot, O., et al. (2019). Sulcal morphology in Alzheimer's disease: An effective marker of diagnosis and cognition. *Neurobiology of Aging*, *84*, 41–49. https://doi.org/10.1016/j.neurobiolaging.2019.07.015, PubMed: 31491594
Borne, L., Rivière, D., Mancip, M., & Mangin, J.-F. (2020). Automatic labeling of cortical sulci using patch- or CNN-based segmentation techniques combined with bottom–up geometric constraints. *Medical Image Analysis*, *62*, 101651. https://doi.org/10.1016/j.media.2020.101651, PubMed: 32163879
Borst, G., Cachia, A., Tissier, C., Ahr, E., Simon, G., & Houdé, O. (2016). Early cerebral constraints on reading skills in school-age children: An MRI study. *Mind, Brain and Education*, *10*, 47–54. https://doi.org/10.1111/mbe.12098
Borst, G., Cachia, A., Vidal, J., Simon, G., Fischer, C., Pineau, A., et al. (2014). Folding of the anterior cingulate cortex partially explains inhibitory control during childhood: A longitudinal study. *Developmental Cognitive Neuroscience*, *9*, 126–135. https://doi.org/10.1016/j.dcn.2014.02.006, PubMed: 24642370
Brodmann, K. (1909). *Vergleichende Lokalisationslehre der Grossbirnrinde in ihren Prinzipien dargestellt auf Grund des Zellenbaues von Dr. K. Brodmann*. J.A. Barth. https://play.google.com/store/books/details?id=Qw5KQwAACAAJ
Bunge, S. A., Helskog, E. H., & Wendelken, C. (2009). Left, but not right, rostrolateral prefrontal cortex meets a stringent test of the relational integration hypothesis. *Neuroimage*, *46*, 338–342. https://doi.org/10.1016/j.neuroimage.2009.01.064, PubMed: 19457362
Cachia, A., Borst, G., Jardri, R., Raznahan, A., Murray, G. K., Mangin, J.-F., et al. (2021). Towards deciphering the fetal foundation of normal cognition and cognitive symptoms from sulcation of the cortex. *Frontiers in Neuroanatomy*, *15*, 712862. https://doi.org/10.3389/fnana.2021.712862, PubMed: 34650408
Cachia, A., Borst, G., Vidal, J., Fischer, C., Pineau, A., Mangin, J.-F., et al. (2014). The shape of the ACC contributes to cognitive control efficiency in preschoolers. *Journal of Cognitive Neuroscience*, *26*, 96–106. https://doi.org/10.1162/jocn_a_00459, PubMed: 23915057
Chi, J. G., Dooling, E. C., & Gilles, F. H. (1977). Gyral development of the human brain. *Annals of Neurology*, *1*, 86–93. https://doi.org/10.1002/ana.410010109
Christoff, K., & Gabrieli, J. D. E. (2000). The frontopolar cortex and human cognition: Evidence for a rostrocaudal hierarchical organization within the human prefrontal cortex. *Psychobiology*, *28*, 168–186. https://doi.org/10.3758/BF03331976
Christoff, K., Prabhakaran, V., Dorfman, J., Zhao, Z., Kroger, J. K., Holyoak, K. J., et al. (2001). Rostrolateral prefrontal cortex involvement in relational integration during reasoning. *Neuroimage*, *14*, 1136–1149. https://doi.org/10.1006/nimg.2001.0922, PubMed: 11697945
Crosson, B., Sadek, J. R., Bobholz, J. A., Gökçay, D., Mohr, C. M., Leonard, C. M., et al. (1999). Activity in the paracingulate and cingulate sulci during word generation: An fMRI study of functional anatomy. *Cerebral Cortex*, *9*, 307–316. https://doi.org/10.1093/cercor/9.4.307, PubMed: 10426410
Cunningham, D. J. (1892). *Contribution to the surface anatomy of the cerebral hemispheres*. Academy House. https://play.google.com/store/books/details?id=t4VCAQAAIAAJ
Dale, A. M., Fischl, B., & Sereno, M. I. (1999). Cortical surface-based analysis. I. Segmentation and surface reconstruction. *Neuroimage*, *9*, 179–194. https://doi.org/10.1006/nimg.1998.0395
Demirtaş, M., Burt, J. B., Helmer, M., Ji, J. L., Adkinson, B. D., Glasser, M. F., et al. (2019). Hierarchical heterogeneity across human cortex shapes large-scale neural dynamics. *Neuron*, *101*, 1181–1194. https://doi.org/10.1016/j.neuron.2019.01.017, PubMed: 30744986
Dworetsky, A., Seitzman, B. A., Adeyemo, B., Neta, M., Coalson, R. S., Petersen, S. E., et al. (2021). Probabilistic mapping of human functional brain networks identifies regions of high group consensus. *Neuroimage*, *237*, 118164. https://doi.org/10.1016/j.neuroimage.2021.118164, PubMed: 34000397
Fan, L., Li, H., Zhuo, J., Zhang, Y., Wang, J., Chen, L., et al. (2016). The human Brainnetome Atlas: A new brain atlas based on connectional architecture. *Cerebral Cortex*, *26*, 3508–3526. https://doi.org/10.1093/cercor/bhw157, PubMed: 27230218
Felleman, D. J., & Van Essen, D. C. (1991). Distributed hierarchical processing in the primate cerebral cortex. *Cerebral Cortex*, *1*, 1–47. https://doi.org/10.1093/cercor/1.1.1-a
Fischl, B., & Dale, A. M. (2000). Measuring the thickness of the human cerebral cortex from magnetic resonance images. *Proceedings of the National Academy of Sciences, U.S.A.*, *97*, 11050–11055. https://doi.org/10.1073/pnas.200033797, PubMed: 10984517
Fischl, B., Sereno, M. I., & Dale, A. M. (1999). Cortical surface-based analysis. II: Inflation, flattening, and a surface-based coordinate system. *Neuroimage*, *9*, 195–207. https://doi.org/10.1006/nimg.1998.0396
Fischl, B., Sereno, M. I., Tootell, R. B., & Dale, A. M. (1999). High-resolution intersubject averaging and a coordinate system for the cortical surface. *Human Brain Mapping*, *8*, 272–284. https://doi.org/10.1002/(sici)1097-0193(1999)8:4<272::aid-hbm10>3.0.co;2-4, PubMed: 10619420
Foit, N. A., Yung, S., Lee, H. M., Bernasconi, A., Bernasconi, N., & Hong, S.-J. (2022). A whole-brain 3D myeloarchitectonic atlas: Mapping the Vogt–Vogt legacy to the cortical surface. *Neuroimage*, *263*, 119617. https://doi.org/10.1016/j.neuroimage.2022.119617, PubMed: 36084859
Fornito, A., Wood, S. J., Whittle, S., Fuller, J., Adamson, C., Saling, M. M., et al. (2008). Variability of the paracingulate sulcus and morphometry of the medial frontal cortex: Associations with cortical thickness, surface area, volume, and sulcal depth. *Human Brain Mapping*, *29*, 222–236. https://doi.org/10.1002/hbm.20381, PubMed: 17497626
Fornito, A., Yücel, M., Wood, S. J., Proffitt, T., McGorry, P. D., Velakoulis, D., et al. (2006). Morphology of the paracingulate sulcus and executive cognition in schizophrenia. *Schizophrenia Research*, *88*, 192–197. https://doi.org/10.1016/j.schres.2006.06.034, PubMed: 16893628
Fornito, A., Yücel, M., Wood, S., Stuart, G. W., Buchanan, J.-A., Proffitt, T., et al. (2004). Individual differences in anterior cingulate/paracingulate morphology are related to executive

functions in healthy males. *Cerebral Cortex*, *14*, 424–431. https://doi.org/10.1093/cercor/bhh004, PubMed: 15028646
Garrison, J. R., Fernyhough, C., McCarthy-Jones, S., Haggard, M., Australian Schizophrenia Research Bank., & Simons, J. S. (2015). Paracingulate sulcus morphology is associated with hallucinations in the human brain. *Nature Communications*, *6*, 8956. https://doi.org/10.1038/ncomms9956, PubMed: 26573408
Glasser, M. F., Coalson, T. S., Robinson, E. C., Hacker, C. D., Harwell, J., Yacoub, E., et al. (2016). A multi-modal parcellation of human cerebral cortex. *Nature*, *536*, 171–178. https://doi.org/10.1038/nature18933, PubMed: 27437579
Glasser, M. F., Sotiropoulos, S. N., Wilson, J. A., Coalson, T. S., Fischl, B., Andersson, J. L., et al. (2013). The minimal preprocessing pipelines for the Human Connectome Project. *Neuroimage*, *80*, 105–124. https://doi.org/10.1016/j.neuroimage.2013.04.127, PubMed: 23668970
Glasser, M. F., & Van Essen, D. C. (2011). Mapping human cortical areas in vivo based on myelin content as revealed by T1- and T2-weighted MRI. *Journal of Neuroscience*, *31*, 11597–11616. https://doi.org/10.1523/JNEUROSCI.2180-11.2011, PubMed: 21832190
Gordon, E. M., Laumann, T. O., Adeyemo, B., Gilmore, A. W., Nelson, S. M., Dosenbach, N. U. F., et al. (2017). Individual-specific features of brain systems identified with resting state functional correlations. *Neuroimage*, *146*, 918–939. https://doi.org/10.1016/j.neuroimage.2016.08.032, PubMed: 27640749
Gordon, E. M., Laumann, T. O., Gilmore, A. W., Newbold, D. J., Greene, D. J., Berg, J. J., et al. (2017). Precision functional mapping of individual human brains. *Neuron*, *95*, 791–807. https://doi.org/10.1016/j.neuron.2017.07.011, PubMed: 28757305
Gratton, C., Nelson, S. M., & Gordon, E. M. (2022). Brain–behavior correlations: Two paths toward reliability [review of brain–behavior correlations: Two paths toward reliability]. *Neuron*, *110*, 1446–1449. https://doi.org/10.1016/j.neuron.2022.04.018, PubMed: 35512638
Green, A. E., Fugelsang, J. A., Kraemer, D. J. M., Shamosh, N. A., & Dunbar, K. N. (2006). Frontopolar cortex mediates abstract integration in analogy. *Brain Research*, *1096*, 125–137. https://doi.org/10.1016/j.brainres.2006.04.024, PubMed: 16750818
Green, A. E., Kraemer, D. J. M., Fugelsang, J. A., Gray, J. R., & Dunbar, K. N. (2010). Connecting long distance: Semantic distance in analogical reasoning modulates frontopolar cortex activity. *Cerebral Cortex*, *20*, 70–76. https://doi.org/10.1093/cercor/bhp081, PubMed: 19383937
Hartogsveld, B., Bramson, B., Vijayakumar, S., van Campen, A. D., Marques, J. P., Roelofs, K., et al. (2018). Lateral frontal pole and relational processing: Activation patterns and connectivity profile. *Behavioural Brain Research*, *355*, 2–11. https://doi.org/10.1016/j.bbr.2017.08.003, PubMed: 28811179
Hathaway, C. B., Voorhies, W. I., Sathishkumar, N., Mittal, C., Yao, J. K., Miller, J. A., et al. (2023). Defining putative tertiary sulci in lateral prefrontal cortex in chimpanzees using human predictions. *Brain Structure & Function*. https://doi.org/10.1007/s00429-023-02638-7, PubMed: 37195311
Hobeika, L., Diard-Detoeuf, C., Garcin, B., Levy, R., & Volle, E. (2016). General and specialized brain correlates for analogical reasoning: A meta-analysis of functional imaging studies. *Human Brain Mapping*, *37*, 1953–1969. https://doi.org/10.1002/hbm.23149, PubMed: 27012301
Holyoak, K. J., & Monti, M. M. (2021). Relational integration in the human brain: A review and synthesis. In. *Journal of Cognitive Neuroscience*, *33*, 341–356. https://doi.org/10.1162/jocn_a_01619, PubMed: 32762521
Hopkins, W. D., Procyk, E., Petrides, M., Schapiro, S. J., Mareno, M. C., & Amiez, C. (2021). Sulcal morphology in cingulate cortex is associated with voluntary oro-facial motor control and gestural communication in chimpanzees (pan troglodytes). *Cerebral Cortex*, *31*, 2845–2854. https://doi.org/10.1093/cercor/bhaa392, PubMed: 33447847
Im, K. (2021). Cortical sulci in the human fetal brain and development. In *Factors affecting neurodevelopment* (pp. 359–369). Academic Press. https://doi.org/10.1016/b978-0-12-817986-4.00031-6
Im, K., & Grant, P. E. (2019). Sulcal pits and patterns in developing human brains. *Neuroimage*, *185*, 881–890. https://doi.org/10.1016/j.neuroimage.2018.03.057, PubMed: 29601953
Kaas, J. H. (1997). Topographic maps are fundamental to sensory processing. *Brain Research Bulletin*, *44*, 107–112. https://doi.org/10.1016/s0361-9230(97)00094-4
Klein, D., Rotarska-Jagiela, A., Genc, E., Sritharan, S., Mohr, H., Roux, F., et al. (2014). Adolescent brain maturation and cortical folding: Evidence for reductions in gyrification. *PLoS One*, *9*, e84914. https://doi.org/10.1371/journal.pone.0084914, PubMed: 24454765
Koechlin, E., Basso, G., Pietrini, P., Panzer, S., & Grafman, J. (1999). The role of the anterior prefrontal cortex in human cognition. *Nature*, *399*, 148–151. https://doi.org/10.1038/20178
Kong, R., Li, J., Orban, C., Sabuncu, M. R., Liu, H., Schaefer, A., et al. (2019). Spatial topography of individual-specific cortical networks predicts human cognition, personality, and emotion. *Cerebral Cortex*, *29*, 2533–2551. https://doi.org/10.1093/cercor/bhy123, PubMed: 29878084
Kong, R., Yang, Q., Gordon, E., Xue, A., Yan, X., Orban, C., et al. (2021). Individual-specific areal-level parcellations improve functional connectivity prediction of behavior. *Cerebral Cortex*, *31*, 4477–4500. https://doi.org/10.1093/cercor/bhab101, PubMed: 33942058
Levy, R., & Goldman-Rakic, P. S. (2000). Segregation of working memory functions within the dorsolateral prefrontal cortex. *Experimental Brain Research*, *133*, 23–32. https://doi.org/10.1007/s002210000397, PubMed: 10933207
Li, Y., Sescousse, G., Amiez, C., & Dreher, J.-C. (2015). Local morphology predicts functional organization of experienced value signals in the human orbitofrontal cortex. *Journal of Neuroscience*, *35*, 1648–1658. https://doi.org/10.1523/JNEUROSCI.3058-14.2015, PubMed: 25632140
Li, M., Wang, D., Ren, J., Langs, G., Stoecklein, S., Brennan, B. P., et al. (2019). Performing group-level functional image analyses based on homologous functional regions mapped in individuals. *PLoS Biology*, *17*, e2007032. https://doi.org/10.1371/journal.pbio.2007032, PubMed: 30908490
Li, X., Zhang, S., Jiang, X., Zhang, S., Han, J., Guo, L., et al. (2022). Cortical development coupling between surface area and sulcal depth on macaque brains. *Brain Structure & Function*, *227*, 1013–1029. https://doi.org/10.1007/s00429-021-02444-z, PubMed: 34989870
Lopez-Persem, A., Verhagen, L., Amiez, C., Petrides, M., & Sallet, J. (2019). The human ventromedial prefrontal cortex: Sulcal morphology and its influence on functional organization. *Journal of Neuroscience*, *39*, 3627–3639. https://doi.org/10.1523/JNEUROSCI.2060-18.2019, PubMed: 30833514
Lyu, I., Bao, S., Hao, L., Yao, J., Miller, J. A., Voorhies, W., et al. (2021). Labeling lateral prefrontal sulci using spherical data augmentation and context-aware training. *Neuroimage*, *229*, 117758. https://doi.org/10.1016/j.neuroimage.2021.117758, PubMed: 33497773
Madan, C. R. (2019). Robust estimation of sulcal morphology. *Brain Informatics*, *6*, 5. https://doi.org/10.1186/s40708-019-0098-1, PubMed: 31187294
Malikovic, A., Vucetic, B., Milisavljevic, M., Tosevski, J., Sazdanovic, P., Milojevic, B., et al. (2012). Occipital sulci of

the human brain: Variability and morphometry. *Anatomical Science International*, *87*, 61–70. https://doi.org/10.1007/s12565-011-0118-6, PubMed: 21993979

Meng, Y., Li, G., Lin, W., Gilmore, J. H., & Shen, D. (2014). Spatial distribution and longitudinal development of deep cortical sulcal landmarks in infants. *Neuroimage*, *100*, 206–218. https://doi.org/10.1016/j.neuroimage.2014.06.004, PubMed: 24945660

Miller, J. A., D'Esposito, M., & Weiner, K. S. (2021). Using tertiary sulci to map the "cognitive globe" of prefrontal cortex. *Journal of Cognitive Neuroscience*, *33*, 1698–1715. https://doi.org/10.1162/jocn_a_01696, PubMed: 34375416

Miller, J. A., Voorhies, W. I., Li, X., Raghuram, I., Palomero-Gallagher, N., Zilles, K., et al. (2020). Sulcal morphology of ventral temporal cortex is shared between humans and other hominoids. *Scientific Reports*, *10*, 17132. https://doi.org/10.1038/s41598-020-73213-x, PubMed: 33051475

Miller, J. A., Voorhies, W. I., Lurie, D. J., D'Esposito, M., & Weiner, K. S. (2021). Overlooked tertiary sulci serve as a meso-scale link between microstructural and functional properties of human lateral prefrontal cortex. *Journal of Neuroscience*, *41*, 2229–2244. https://doi.org/10.1523/JNEUROSCI.2362-20.2021, PubMed: 33478989

Nakamura, M., Nestor, P. G., & Shenton, M. E. (2020). Orbitofrontal sulcogyral pattern as a transdiagnostic trait marker of early neurodevelopment in the social brain. *Clinical EEG and Neuroscience*, *51*, 275–284. https://doi.org/10.1177/1550059420904180, PubMed: 32028799

Natu, V. S., Arcaro, M. J., Barnett, M. A., Gomez, J., Livingstone, M., Grill-Spector, K., et al. (2021). Sulcal depth in the medial ventral temporal cortex predicts the location of a place-selective region in macaques, children, and adults. *Cerebral Cortex*, *31*, 48–61. https://doi.org/10.1093/cercor/bhaa203, PubMed: 32954410

Natu, V. S., Gomez, J., Barnett, M., Jeska, B., Kirilina, E., Jaeger, C., et al. (2019). Apparent thinning of human visual cortex during childhood is associated with myelination. *Proceedings of the National Academy of Sciences, U.S.A.*, *116*, 20750–20759. https://doi.org/10.1073/pnas.1904931116, PubMed: 31548375

Nee, D. E., & D'Esposito, M. (2016). The hierarchical organization of the lateral prefrontal cortex. *eLife*, *5*, e12112. https://doi.org/10.7554/eLife.12112, PubMed: 26999822

Paus, T., Tomaiuolo, F., Otaky, N., MacDonald, D., Petrides, M., Atlas, J., et al. (1996). Human cingulate and paracingulate sulci: Pattern, variability, asymmetry, and probabilistic map. *Cerebral Cortex*, *6*, 207–214. https://doi.org/10.1093/cercor/6.2.207, PubMed: 8670651

Petrides, M. (2005). Lateral prefrontal cortex: Architectonic and functional organization. *Philosophical Transactions of the Royal Society of London, Series B, Biological Sciences*, *360*, 781–795. https://doi.org/10.1098/rstb.2005.1631, PubMed: 15937012

Petrides, M. (2013). *Neuroanatomy of language regions of the human brain*. Academic Press. https://play.google.com/store/books/details?id=DYlqAAAAQBAJ

Petrides, M. (2019). *Atlas of the morphology of the human cerebral cortex on the average MNI brain*. Academic Press. https://play.google.com/store/books/details?id=qeWcBAAAQBAJ

Ramnani, N., & Owen, A. M. (2004). Anterior prefrontal cortex: Insights into function from anatomy and neuroimaging. *Nature Reviews Neuroscience*, *5*, 184–194. https://doi.org/10.1038/nrn1343

Raznahan, A., Shaw, P., Lalonde, F., Stockman, M., Wallace, G. L., Greenstein, D., et al. (2011). How does your cortex grow? *Journal of Neuroscience*, *31*, 7174–7177. https://doi.org/10.1523/JNEUROSCI.0054-11.2011, PubMed: 21562281

Rollins, C. P. E., Garrison, J. R., Arribas, M., Seyedsalehi, A., Li, Z., Chan, R. C. K., et al. (2020). Evidence in cortical folding patterns for prenatal predispositions to hallucinations in schizophrenia. *Translational Psychiatry*, *10*, 387. https://doi.org/10.1038/s41398-020-01075-y, PubMed: 33159044

Rosenkilde, C. E. (1979). Functional heterogeneity of the prefrontal cortex in the monkey: A review. *Behavioral and Neural Biology*, *25*, 301–345. https://doi.org/10.1016/s0163-1047(79)90404-7

Sanides, F. (1964). Structure and function of the human frontal lobe. *Neuropsychologia*, *2*, 209–219. https://doi.org/10.1016/0028-3932(64)90005-3

Scholtens, L. H., de Reus, M. A., de Lange, S. C., Schmidt, R., & van den Heuvel, M. P. (2018). An MRI Von Economo–Koskinas atlas. *Neuroimage*, *170*, 249–256. https://doi.org/10.1016/j.neuroimage.2016.12.069, PubMed: 28040542

Seitzman, B. A., Gratton, C., Laumann, T. O., Gordon, E. M., Adeyemo, B., Dworetsky, A., et al. (2019). Trait-like variants in human functional brain networks. *Proceedings of the National Academy of Sciences, U.S.A.*, *116*, 22851–22861. https://doi.org/10.1073/pnas.1902932116, PubMed: 31611415

Shams, Z., Norris, D. G., & Marques, J. P. (2019). A comparison of in vivo MRI based cortical myelin mapping using T1w/T2w and R1 mapping at 3T. *PLoS One*, *14*, e0218089. https://doi.org/10.1371/journal.pone.0218089, PubMed: 31269041

Smith, R., Keramatian, K., & Christoff, K. (2007). Localizing the rostrolateral prefrontal cortex at the individual level. *Neuroimage*, *36*, 1387–1396. https://doi.org/10.1016/j.neuroimage.2007.04.032, PubMed: 17532648

Stuss, D. T., & Knight, R. T. (2013). *Principles of frontal lobe function*. Oxford University Press. https://play.google.com/store/books/details?id=GHrAhCMGj2EC, https://doi.org/10.1093/med/9780199837755.001.0001

Troiani, V., Dougherty, C. C., Michael, A. M., & Olson, I. R. (2016). Characterization of face-selective patches in orbitofrontal cortex. *Frontiers in Human Neuroscience*, *10*, 279. https://doi.org/10.3389/fnhum.2016.00279, PubMed: 27378880

Troiani, V., Patti, M. A., & Adamson, K. (2020). The use of the orbitofrontal H-sulcus as a reference frame for value signals. *European Journal of Neuroscience*, *51*, 1928–1943. https://doi.org/10.1111/ejn.14590, PubMed: 31605399

Urbanski, M., Bréchemier, M.-L., Garcin, B., Bendetowicz, D., Thiebaut de Schotten, M., Foulon, C., et al. (2016). Reasoning by analogy requires the left frontal pole: Lesion-deficit mapping and clinical implications. *Brain*, *139*, 1783–1799. https://doi.org/10.1093/brain/aww072

Vallejo-Azar, M. N., Alba-Ferrara, L., Bouzigues, A., Princich, J. P., Markov, M., Bendersky, M., et al. (2022). Influence of accessory sulci of the frontoparietal operculum on gray matter quantification. *Frontiers in Neuroanatomy*, *16*, 1022758. https://doi.org/10.3389/fnana.2022.1022758, PubMed: 37089581

Van Essen, D. C. (2003). Organization of Visual Areas in macaque and human cerebral cortex. In L. Chalupa & J. Werner (Ed.), *Visual neurosciences*. https://www.cns.nyu.edu/csh/csh04/Articles/Vanessen-03.pdf

Van Essen, D. C. (2005). A population-average, landmark- and surface-based (PALS) atlas of human cerebral cortex. *Neuroimage*, *28*, 635–662. https://doi.org/10.1016/j.neuroimage.2005.06.058, PubMed: 16172003

Vandekar, S. N., Shinohara, R. T., Raznahan, A., Roalf, D. R., Ross, M., DeLeo, N., et al. (2015). Topologically dissociable patterns of development of the human cerebral cortex. *Journal of Neuroscience*, *35*, 599–609. https://doi.org/10.1523/JNEUROSCI.3628-14.2015, PubMed: 25589754

Vendetti, M. S., & Bunge, S. A. (2014). Evolutionary and developmental changes in the lateral frontoparietal network: A little goes a long way for higher-level cognition. *Neuron*, *84*, 906–917. https://doi.org/10.1016/j.neuron.2014.09.035, PubMed: 25475185

Vogt, C., & Vogt, O. (1919). *Allgemeine Ergebnisse unserer Hirnforschung*. J.A. Barth. https://play.google.com/store/books/details?id=BJcXAAAAYAAJ

von Economo, C. F., & Koskinas, G. N. (1925). *Die cytoarchitektonik der hirnrinde des erwachsenen menschen*. J. Springer. https://play.google.com/store/books/details?id=2DVBAAAAYAAJ

Voorhies, W. I., Miller, J. A., Yao, J. K., Bunge, S. A., & Weiner, K. S. (2021). Cognitive insights from tertiary sulci in prefrontal cortex. *Nature Communications*, *12*, 5122. https://doi.org/10.1038/s41467-021-25162-w, PubMed: 34433806

Weiner, K. S. (2019). The mid-fusiform sulcus (sulcus sagittalis gyri fusiformis). *Anatomical Record*, *302*, 1491–1503. https://doi.org/10.1002/ar.24041, PubMed: 30471211

Weiner, K. S., Golarai, G., Caspers, J., Chuapoco, M. R., Mohlberg, H., Zilles, K., et al. (2014). The mid-fusiform sulcus: A landmark identifying both cytoarchitectonic and functional divisions of human ventral temporal cortex. *Neuroimage*, *84*, 453–465. https://doi.org/10.1016/j.neuroimage.2013.08.068, PubMed: 24021838

Weiner, K. S., Natu, V. S., & Grill-Spector, K. (2018). On object selectivity and the anatomy of the human fusiform gyrus. *Neuroimage*, *173*, 604–609. https://doi.org/10.1016/j.neuroimage.2018.02.040, PubMed: 29471101

Welker, W. (1990). Why does cerebral cortex fissure and fold? In E. G. Jones & A. Peters (Eds.), *Cerebral cortex: Comparative structure and evolution of cerebral cortex, part II* (pp. 3–136). Springer. https://doi.org/10.1007/978-1-4615-3824-0_1

Wendelken, C., Ferrer, E., Ghetti, S., Bailey, S. K., Cutting, L., & Bunge, S. A. (2017). Frontoparietal structural connectivity in childhood predicts development of functional connectivity and reasoning ability: A large-scale longitudinal investigation. *Journal of Neuroscience*, *37*, 8549–8558. https://doi.org/10.1523/JNEUROSCI.3726-16.2017, PubMed: 28821657

Wendelken, C., Nakhabenko, D., Donohue, S. E., Carter, C. S., & Bunge, S. A. (2008). "Brain is to thought as stomach is to ??": Investigating the role of rostrolateral prefrontal cortex in relational reasoning. *Journal of Cognitive Neuroscience*, *20*, 682–693. https://doi.org/10.1162/jocn.2008.20055, PubMed: 18052787

Westphal, A. J., Chow, T. E., Ngoy, C., Zuo, X., Liao, V., Storozuk, L. A., et al. (2019). Anodal transcranial direct current stimulation to the left rostrolateral prefrontal cortex selectively improves source memory retrieval. *Journal of Cognitive Neuroscience*, *31*, 1380–1391. https://doi.org/10.1162/jocn_a_01421, PubMed: 31059351

Westphal, A. J., Reggente, N., Ito, K. L., & Rissman, J. (2016). Shared and distinct contributions of rostrolateral prefrontal cortex to analogical reasoning and episodic memory retrieval. *Human Brain Mapping*, *37*, 896–912. https://doi.org/10.1002/hbm.23074, PubMed: 26663572

Willbrand, E. H., Ferrer, E., Bunge, S. A., & Weiner, K. S. (2023). Development of human lateral prefrontal sulcal morphology and its relation to reasoning performance. *Journal of Neuroscience*, *43*, 2552–2567. https://doi.org/10.1523/JNEUROSCI.1745-22.2023, PubMed: 36828638

Willbrand, E. H., Jackson, S., Chen, S., Hathaway, C. B., Voorhies, W. I., Bunge, S. A., et al. (2023). Cognitive relevance of an evolutionarily new and variable prefrontal structure. *bioRxiv*. https://doi.org/10.1101/2023.02.10.528061, PubMed: 36798378

Willbrand, E. H., Maboudian, S. A., Kelly, J. P., Parker, B. J., Foster, B. L., & Weiner, K. S. (2023). Sulcal morphology of posteromedial cortex substantially differs between humans and chimpanzees. *Communications Biology*, *6*, 586. https://doi.org/10.1038/s42003-023-04953-5, PubMed: 37264068

Willbrand, E. H., Parker, B. J., Voorhies, W. I., Miller, J. A., Lyu, I., Hallock, T., et al. (2022). Uncovering a tripartite landmark in posterior cingulate cortex. *Science Advances*, *8*, eabn9516. https://doi.org/10.1126/sciadv.abn9516, PubMed: 36070384

Willbrand, E. H., Voorhies, W. I., Yao, J. K., Weiner, K. S., & Bunge, S. A. (2022). Presence or absence of a prefrontal sulcus is linked to reasoning performance during child development. *Brain Structure & Function*, *227*, 2543–2551. https://doi.org/10.1007/s00429-022-02539-1, PubMed: 35932310

Yao, J. K., Voorhies, W. I., Miller, J. A., Bunge, S. A., & Weiner, K. S. (2022). Sulcal depth in prefrontal cortex: A novel predictor of working memory performance. *Cerebral Cortex*, *33*, 1799–1813. https://doi.org/10.1093/cercor/bhac173, PubMed: 35589102

Zilles, K. (2018). Brodmann: A pioneer of human brain mapping-his impact on concepts of cortical organization. *Brain*, *141*, 3262–3278. https://doi.org/10.1093/brain/awy273, PubMed: 30358817

Zlatkina, V., Amiez, C., & Petrides, M. (2016). The postcentral sulcal complex and the transverse postcentral sulcus and their relation to sensorimotor functional organization. *European Journal of Neuroscience*, *43*, 1268–1283. https://doi.org/10.1111/ejn.13049, PubMed: 26296305